CHAPTER 10

Theoretical Investigation of Atmospheric Oxidation of Biogenic Hydrocarbons: A Critical Review

Jun Zhao* and **Renyi Zhang[1*]**

Contents

1. INTRODUCTION

Non-methane hydrocarbons (NMHCs) are emitted into the atmosphere from natural and anthropogenic sources and represent an important fraction of volatile organic compounds (VOCs) in the atmosphere [1–4]. Globally, the annual emission of VOCs from biogenic sources (primarily from vegetation) is estimated to be about 1150 Tg C, more than half of which (~55%) is isoprene and monoterpenes [1]. Biogenic VOCs dominate over the anthropogenic counterparts by an order magnitude, which only account for ~10% of the total VOC budget, although the anthropogenic fraction is higher in urban atmosphere (~20–30%) [5,6].

Once emitted into the atmosphere, the VOCs involve in several chemical and physical processes, leading to transformation and removal from the atmosphere [6]. Chemical transformation of VOCs in the atmosphere occurs in sev-

* Department of Atmospheric Sciences and Department of Chemistry, Texas A&M University, College Station, TX 77843, USA
[1] Corresponding author. Fax: +1 979 862 4466. E-mail: zhang@ariel.met.tamu.edu

Advances in Quantum Chemistry, Vol. 55
ISSN 0065-3276, DOI: 10.1016/S0065-3276(07)00210-9

eral ways including photolysis, thermal decomposition, and most importantly the reactions with atmospheric oxidants, which include hydroxyl radical OH, nitrate radical NO_3, ozone O_3, and halogen atoms (e.g., Cl, Br or I) [5,6]. Physical removal of VOCs includes dry deposition and wet deposition, eventually depositing them to the Earth's surface. The lifetimes of VOCs in the troposphere depend on their reactivity and the abundance of oxidants, ranging from seconds to years [4–6]. In particular, photochemical oxidation of hydrocarbons in the atmosphere leads to ozone, toxic compound, and secondary organic aerosol (SOA) formation, with major implications for air quality, human health, and climate change [7–10].

Oxidation of hydrocarbons has long been considered as a fundamental problem to atmospheric chemists, both from experimental and theoretical points of view, because of the inherent complexity. The reaction kinetics and mechanism of atmospheric hydrocarbons have been the focuses of numerous researches in both experimental and theoretical aspects. Although advances have been made in elucidation of the VOC oxidation mechanisms, large uncertainty and tremendous numbers of unexplored reactions still remain. Several review articles on the atmospheric degeneration of VOCs have been published [4,11–14]. In this review, recent advances in the application of theoretical methods to the atmospheric oxidation of biogenic hydrocarbons are discussed. We will introduce the backgrounds on the quantum chemical calculations and kinetic rate theories, recent progress on theoretical studies of isoprene and α-, β-pinenes, and studies on other monoterpenes and sesquiterpenes.

2. THEORETICAL APPROACHES IN ATMOSPHERIC HYDROCARBON OXIDATION RESEARCH

The chemistry of atmospheric hydrocarbon oxidation is highly complex. Despite nearly decades of research conducted in this field, there remains an inadequate understanding of this class of reaction mechanisms at the fundamental molecular level. Oxidation of hydrocarbons is initiated by various radical species and proceeds through multiple reaction pathways and steps. At each stage of the chain reactions intermediate organic radicals are produced to propagate or terminate the oxidation process, and the organic radicals play a key role in determining the final product distribution. Currently, the detailed kinetics and mechanism of hydrocarbon oxidation remain highly uncertain, hindering numerical simulations of the VOC oxidation in atmospheric chemical transport models [15]. Most of organic intermediate radicals arising from oxidation of atmospherically important hydrocarbons have not been detected directly in the gas phase. While the enormous chemical complexity in the hydrocarbon oxidation poses an insurmountable obstacle for current analytical techniques in resolving the intermediate steps and isomeric branching, theoretical calculations promise great advantages in providing insights into the intermediate processes.

With rapid development of computer techniques and algorithms to improve the computational capacities and efficiencies over the last few decades, quantum chemical calculations have been employed as a useful and accessible tool

in the hydrocarbon oxidation research and demonstrated for the important roles in elucidating the oxidation mechanisms of atmospheric hydrocarbons. Quantum chemical calculations utilize a variety of computational methods, ranging from semi-empirical, density functional methods to *ab initio* calculations [16]. The latter approaches are extensively employed in the field of chemistry of hydrocarbon oxidation, which involves primarily gas-phase reactions. Density functional methods have been widely adopted in many fields of chemistry by merit of their relatively moderate computational cost and high accuracy [17,18]. Geometries obtained from density functional methods, especially those employing hybrid functionals (e.g. B3LYP, B3PW91) are often as reliable as those from Moller–Plesset perturbation (MP2) theory. However, density functional methods in some cases fail to provide accurate energetic information. For example, it has been shown density functional methods fail to predict the potential energy surface in some reaction systems (e.g., in the case of a van der Waals complex and loose transition state) [19–21]. Hence, high levels of *ab initio* calculations are required to obtain more accurate reaction energies and activation energies and other thermochemical parameters. Methods incorporating high level of electron correlation (e.g., MP2 method, CCSD(T) and QCISD(T)) have been widely used in the hydrocarbon oxidation community [22–27]. In recent years, composite methods (e.g., Gaussian series of theory (G1, G2, G3 and G4) and the complete basis set (CBS)) have been applied to the hydrocarbon oxidation and have provided intriguing and highly accurate thermochemical data (e.g., bonding energy, heat of formation and proton affinity) [28,29]. Those methods are based on a well-defined single-configuration wave function. It should be pointed out that one can obtain the multi-reference character of a molecular system by analyzing the single-configuration wave function using the T1 diagnostic method. For example, the single reference method (e.g., CCSD) is not reliable if the T1 diagnostic value of the wave function is larger than 0.044 [30,31]. Many reaction systems are essential multi-reference configurations so that multi-configuration interaction theories are required to accurately describe the reaction systems. The most efficient approach is the complete active space self-consistent field (CASSCF), which has been applied to investigate the complex oxidation mechanisms of the atmospheric hydrocarbons [32–34]. The choice of level of theory and basis set in quantum chemical calculations requires consideration of the best compromise between the accuracy and computational cost. Since the hydrocarbon oxidation systems contain both open and close shell species, caution needs to be excised regarding basis set related error and spin contamination, which can be critical factors in many calculations [35]. The above-mentioned methodologies are discussed extensively in the literature [16–18,22–33,36–40].

Chemical kinetic rate methods including conventional transition state theory (TST), canonical variational transition state theory (CVTST) and Rice–Ramsperger–Kassel–Marcus in conjunction with master equation (RRKM/ME) and separate statistical ensemble (SSE) have been successfully applied to the hydrocarbon oxidation. Transition state theory has been developed and employed in many disciplines of chemistry [41–44]. In the atmospheric chemistry field, conventional transition state theory is employed to calculate the high-pressure-limit unimolecular or bimolecular rate constants if a well-defined transition state (i.e., a tight

transition state) exists in the potential energy surface along the reaction coordinate; that is, there exists a surface dividing the reactants from the products and passing through the saddle point of the potential energy surface. The rate constants is expressed by [44]

$$k_{\mathrm{TST}} = \kappa \frac{k_{\mathrm{b}}T}{h} \frac{Q^{\neq}}{Q_{\mathrm{A}}} \exp\left(-\frac{E_{\mathrm{a}}}{RT}\right) \quad \text{(for unimolecular reaction)}, \tag{1}$$

$$k_{\mathrm{TST}} = \kappa \frac{k_{\mathrm{b}}T}{h} \frac{Q^{\neq}}{Q_{\mathrm{A}}Q_{\mathrm{B}}} \exp\left(-\frac{E_{\mathrm{a}}}{RT}\right) \quad \text{(for bimolecular reaction)}, \tag{2}$$

where $Q^{\neq}$ is the partition function of the transition state with the vibrational frequency corresponding to the reaction coordinate removed, Q_{A} and Q_{B} are the partition functions of the reactants. k_{b} and h are Boltzmann constant and the Planck constant, respectively. T is the temperature and κ is the tunneling effect correction factor. The partition functions are calculated from the rotational constants and frequency information by performing the frequency calculations. The activation energy E_{a} is determined from the energy difference between the transition state and the reactants with zero-point energy corrected. If the dividing surface does not pass through the saddle point, a well-defined transition state does not exist (i.e., a loose transition state). The transition state can only be located by varying the dividing surface to minimize the one-way flux coefficient. In this case, the high-pressure limit rate constants are evaluated using CVTST [45,46]. For a bimolecular reaction: $\mathrm{A} + \mathrm{B} \rightarrow \mathrm{AB}$, the unimolecular rate is given by

$$k_{\mathrm{uni}} = \frac{kT}{h} \frac{Q^{\neq}_{AB}}{Q_{AB}} \exp\left(-\frac{\Delta E}{kT}\right), \tag{3}$$

where ΔE is the zero-point corrected transition state energy relative to the separated reactants. The unimolecular rates (k_{uni}) are converted to the bimolecular rates (k_{rec}) via the equilibrium constant,

$$\frac{k_{\mathrm{rec}}}{k_{\mathrm{uni}}} = K_{\mathrm{eq}} = \frac{Q_{\mathrm{AB}}}{Q_{\mathrm{A}}Q_{\mathrm{B}}} \exp\left(\frac{\Delta E'}{kT}\right), \tag{4}$$

where $\Delta E'$ is the zero-point corrected reaction energy. The partition functions in Eqs. (3) and (4) are calculated by treating the rotational and translational motion classically and treating vibrational modes quantum mechanically. Unscaled vibrational frequencies and moments of inertia are taken from the frequency calculations. The conserved modes of the transition state are assumed to assemble the product modes. The dependence of the transitional mode frequencies on reaction coordinate is modeled using [47]

$$\upsilon(r) = \upsilon_0 \exp\left[-a(r - r_{\mathrm{e}})\right] + b, \tag{5}$$

where υ_0 is the vibrational frequency in the reactant molecule, r_{e} is the equilibrium bond distance in the reaction coordinate, b is the sum of the rotational constants of the individual reactant molecule. The coefficient a is a constant which can be determined by performing constrained optimization along the reaction coordinate.

Moments of inertia at fixed geometries are calculated by changing only the bond distance in the reaction coordinate. The potential energy surface along the reaction coordinate is modeled by a Morse function including the centrifugal barrier [48]

$$V(r) = \mathrm{De}\left[1 - \exp\left(-\beta(r - r_\mathrm{e})\right)\right]^2 + B_\mathrm{ext}(r)J(J+1), \tag{6}$$

where D_e is the bond dissociation energy, $B_\mathrm{ext}(r)$ is the external rotational constant determined by assuming that the molecular is a symmetric top, and J is assumed to be the average rotational quantum number of a Boltzmann distribution calculated using the external constant of the molecule at the equilibrium configuration. The β parameter for the Morse function is expressed as $\beta = (2\pi^2\mu/D_\mathrm{e})^{1/2}\nu$, where μ is the reduced mass of the bond atoms, D_e is the bond dissociation energy, ν is the vibrational frequency of the reaction coordinate in parent molecule.

Many hydrocarbon oxidation reactions are strongly exothermic and the excessive internal energy is retained and partitioned over the products, leading to formation of chemically excited intermediated species. The statistical-dynamical master equation in combination with standard RRKM or variational RRKM (vRRKM) theory has been employed to assess the fate of the vibrationally excited species governed by competition between collisional stabilization and consecutive chemical reactions [48–50]. The excited species are stabilized by transferring their energy to the surrounding bath gas. An exponential model is employed to model the collision energy transfer with a specified average energy in the RRKM calculations. An example to illustrate the application of kinetic methods to elucidate the oxidation mechanism of atmospheric hydrocarbons is presented in Figure 10.1, showing the reaction diagram for the OH–isoprene alkoxy radicals formed in the reaction of peroxy radical with NO. The reaction of peroxy radical (RO_2) with NO leads to the formation of a vibrationally excited peroxynitrite (ROONO*) with an internal energy inherited from the thermal reactants [51,52]. The nascent molecular population of the ROONO is described by a shifted thermal distribution [53],

$$f^\mathrm{ROONO}(E) = \frac{W_\mathrm{ROONO}(E - E_{(-x)})\exp[-(E - E_{(-x)})/k_\mathrm{b}T]}{\int_0^\infty W_\mathrm{ROONO}(\varepsilon)\exp(\varepsilon/k_\mathrm{b}T)\,d\varepsilon} \tag{7}$$

for $E \geqslant E_{(-x)}$ with the energy being counted from the ground state of the ROONO. W_ROONO is the sum of the states of the ROONO, $E_{(-x)}$ is the barrier height of the reverse reaction of x. Since the entrance channel is barrierless, a Morse potential including the centrifugal barrier (as mentioned above) can be used to variationally locate the transition states for NO addition to the hydroxyperoxy radical as a function of energy. The collisional energy loss of the ROONO* prior to its dissociation into RO + NO_2 modifies its internal energy distribution to $f^\mathrm{RO}(E)$ at dissociation by assuming only the energy in excess of the activation barrier partitioning statistically between the dissociating fragments [53,54],

$$f^\mathrm{RO}(E) = \frac{\rho_\mathrm{RO}(E)W_\mathrm{RO}(E_\mathrm{tot} - E)}{\int_0^{E_\mathrm{tot}} \rho_\mathrm{RO}(\varepsilon)W_\mathrm{RO}(E_\mathrm{tot} - \varepsilon)\,d\varepsilon}, \tag{8}$$

where E_{tot} is the overall disposable energy and ρ_{RO} is the density of states of the RO, that is the number of electron states per unit energy interval. The dissociation of the ROONO* and partitioning of the disposable excess energy over two fragments ($\text{RO} + \text{NO}_2$) and over the degrees of freedom of their relative motion can be calculated according to the separate statistical ensemble (SSE) theory [55,56]. The probability of formation of RO radical with in a given vibrational (rotational) level i is given by [55,56]

$$P_{\text{RO}_i}^{E_{\text{tot}}}(E_{\text{RO}}) = \left(N_{\text{RO}_i}(E_{\text{RO}}) \int_0^{E_{\text{tot}}-E_{\text{RO}}} \left[N_{\text{NO}_2}(E_{\text{NO}_2}) N_{\text{rel mot}}(E_{\text{tot}} - E_{\text{RO}} - E_{\text{NO}_2}) \right] dE_{\text{NO}_2} \right)$$
$$\times \left(\int_0^{E_{\text{tot}}} \left\{ \left(\sum_i N_{\text{RO}_i}(E_{\text{RO}}) \right) \int_0^{E_{\text{tot}}-E_{\text{RO}}} \left[N_{\text{NO}_2}(E_{\text{NO}_2}) N_{\text{rel mot}} \right. \right. \right.$$
$$\left. \left. \left. \times (E_{\text{tot}} - E_{\text{RO}} - E_{\text{NO}_2}) \right] dE_{\text{NO}_2} \right\} dE_{\text{RO}} \right)^{-1}, \tag{9}$$

where $N_{\text{RO}_i}(E_{\text{RO}})$, $N_{\text{NO}_2}(E_{\text{NO}_2})$, and $N_{\text{rel mot}}(E_{\text{tot}} - E_{\text{RO}} - E_{\text{NO}_2})$ are the density of state of the ith energy level for RO, the density of state of NO_2, and the density of state of relative motion, respectively. For the relative motion, $N_{\text{rel mot}}(E)$ varies with E^2 since the relative motion is treated as unhindered motion which $N(E)$ varies with its degrees freedom y as $E^{(y/2)-1}$.

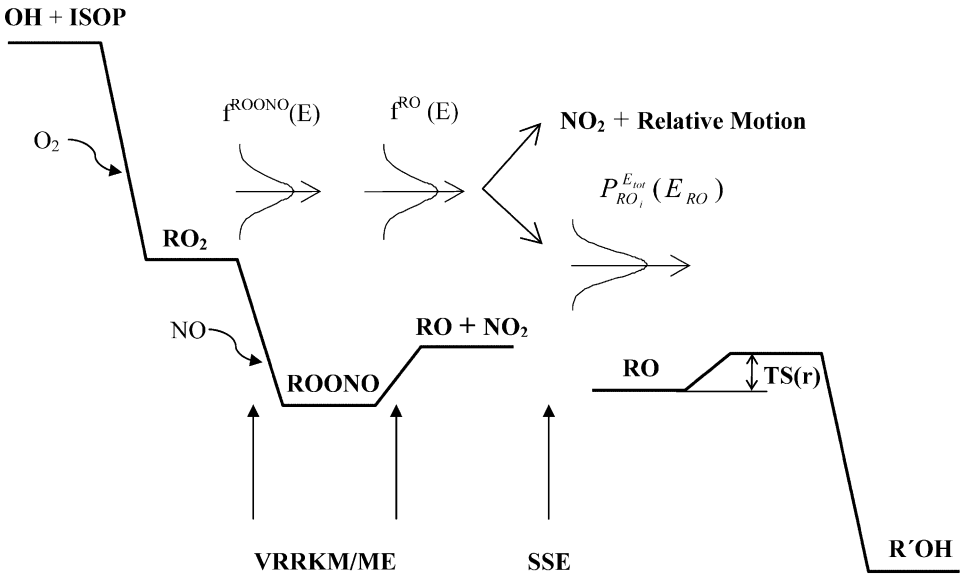

FIGURE 10.1 An example of the application of the kinetic theory to the hydrocarbon oxidation: the potential energy surface of OH-initiated isoprene system.

The microcanonical rate constant at energy E can be expressed using the RRKM theory [48],

$$k_r(E) = \frac{W_r(E - E_{TS(r)})}{h\rho(E)}, \tag{10}$$

where W_r is the sum of states of the transition state for reaction r. The concentration of a relevant species is related to a balance over all gain and loss processes for a given energy level i according to statistical dynamic master equation [48],

$$\frac{dn_i}{dt} = Rf_i - \omega n_i + \sum_i P_{ij} n_j - \sum_l k_{li} n_i, \tag{11}$$

where n_i is the concentration of the species having internal energy E_i, R is the overall formation rate, f_i is the normalized energy distribution, P_{ij} is the energy transfer probability from j to i, k_{li} is the reaction rate constant for pathway l, and ω is the collision frequency. Assuming the steady-state condition, Eq. (11) becomes

$$RF = \left[\omega(I - P) + \sum K_r\right] N^s \equiv JN^s, \tag{12}$$

where the vector/matrix symbols correspond to those in Eq. (11) and I denotes the unit matrix. The steady-state population N^s follows from $N^s = RJ^{-1}F$, and the rate of reaction r is $D_r = \sum(K_r N^s)_i$. The relative yields are then expressed by $Dr/R = \sum(K_r J^{-1} F)_i$, and the stabilization fraction follows from $S/R = 1 - \sum D_r/R$. It should be pointed out that while most of the reactions can be solved using traditional RRKM approach, experimental and theoretical studies have shown that non-RRKM dynamics is important for moderate to large-sized molecules with various barriers for unimolecular dissociation [57,58]. In these cases, non-RRKM behavior needs to be taken into account and direct chemical dynamic simulation is suggested to serve this purpose [58].

3. THEORETICAL INVESTIGATION OF BIOGENIC HYDROCARBON OXIDATION

3.1 Isoprene

Isoprene (2-methyl-1,3-butadiene, CH_2=C(CH_3)–CH=CH_2) is one of the most abundant hydrocarbons emitted by the terrestrial biosphere with a global average production rate of 450 Tg yr^{-1} and is sufficiently reactive to influence oxidation levels over large portions of the continental troposphere [59,60]. An accurate and complete knowledge of the atmospheric chemistry of isoprene is critical to elucidate chemical mechanisms of atmospheric hydrocarbons in urban and regional environments [15]. Atmospheric oxidation reactions of isoprene are initiated by attacks from the atmospheric oxidants, including OH, O_3, NO_3, and halogen atoms.

3.1.1 OH-initiated oxidation

Since isoprene is emitted from vegetation only during daylight hours, the reaction with OH is expected to be the dominant tropospheric removal pathway. The

reaction between isoprene and OH occurs almost entirely by OH addition to the >C=C< bonds, yielding four possible hydroxyalkyl radicals. Under atmospheric conditions, the hydroxyalkyl radicals react primarily with oxygen molecules to form hydroxyalkyl peroxy radicals (RO_2). In the presence of nitric oxide NO, the subsequent reactions of the hydroxyalkyl peroxy radicals lead to the formation of hydroxyalkoxy radicals (RO). Alternatively, a small fraction of peroxy radicals will react with NO to produce hydroxylalkyl nitrates ($RONO_2$). Under low NO_x conditions, the peroxy radicals will undergo permutation reactions (e.g., self reactions and cross reactions) or reaction with HO_2 to produce a variety of products (e.g., hydoxyalkoxy radicals, hydroperoxide, carbonyls, alcohol and carboxylic acids) [61–64]. The dominant tropospheric reaction of β-hydroxyalkoxy radicals is believed to be decomposition, leading to the formation of various oxygenated (e.g., methyl vinyl ketone, methacrolein, 3-methyl furan) and nitrated organic compounds while for δ-hydroxyalkoxy radicals, the isomerization pathway has been shown to be dominant over the decomposition, leading to the formation of hydroxycarbonyls, which have been detected and quantified experimentally [65–68]. Figure 10.2 depicts the mechanistic diagram of the OH-initiated oxidation of isoprene [69].

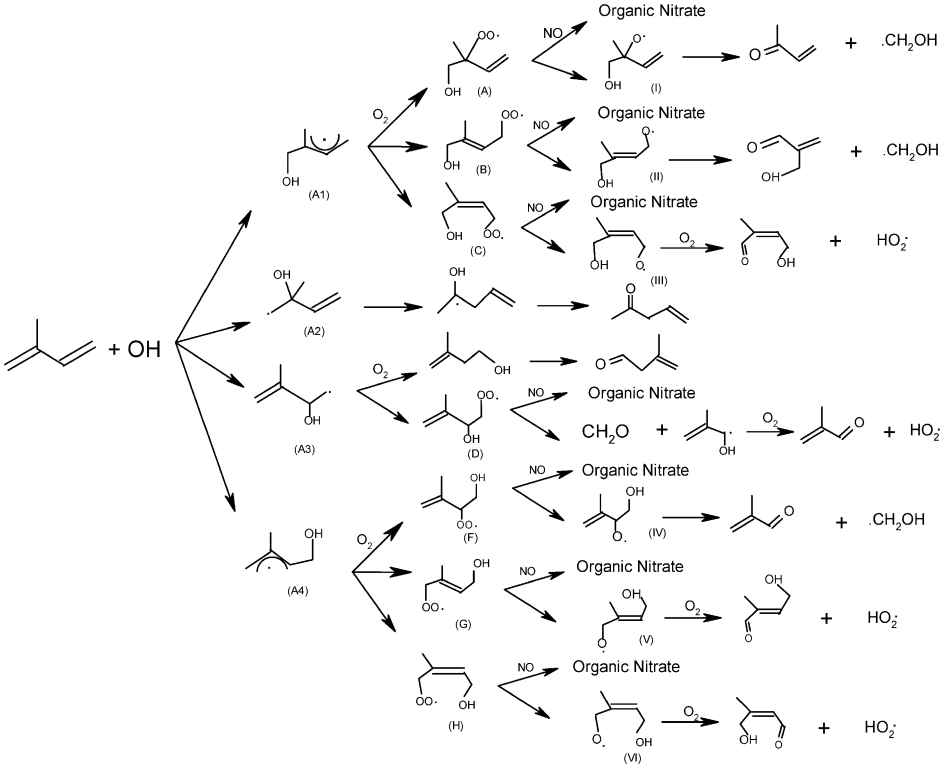

FIGURE 10.2 Mechanistic diagram of OH-initiated isoprene oxidation: detailed reaction pathways and major products.

Systematic theoretical studies of OH–isoprene oxidation have been conducted in recent years. Although the initial step of this reaction is relatively well understood, some discrepancies exist for the potential energy surface of the initial step. In the previous work by Zhang, North, and co-workers (e.g., [51,69–72]), a series of theoretical calculations have been performed to elucidate the mechanisms of the OH–isoprene reactions. Isomeric branching ratios of the initial step have been determined using density functional theory (DFT) and *ab initio* methods coupled to kinetic theories, e.g., CVTST and RRKM/ME. Density functional and *ab initio* methods obtained geometry, frequency and energetic information of the OH–isoprene adducts, which were then incorporated into CVTST to calculate the branching ratios. Four adduct isomers have been globally located along the potential energy surface by gradient corrected density functional theory (DFT) in conjunction with a split valence polarized basis set (B3LYP/6-31G(d,p)). This level of theory has been evaluated for many hydrocarbon oxidation systems and has been shown to be quite robust in geometry optimization and frequency calculations. High levels of *ab initio* methods (e.g., CCSD(T) and MP2 with various basis sets) were then employed to perform single energy calculations to reevaluate the relative energies and activation energies for the relevant reaction systems. A correction factor (CF) term was introduced and defined as the energy difference between the two MP2 levels: MP2/6-311++G(d,p) and MP2/6-31G(d). Hence, the highest level of theory corresponded to CCSD(T)/6-31G(d) + CF for most of *ab initio* calculations. A branching ratio of 0.56:0.02:0.05:0.37 for the isomers A1–A4 is obtained (labeling refers to Figure 10.2) and a high-pressure limit reaction rate of 1.0×10^{-10} cm^{-3} molecule^{-1} s^{-1} is calculated according to the CVTST calculations [70,71]. In addition, the results also show that the inter-conversions (e.g., A1 $\leftrightarrow$ A2 and A3 $\leftrightarrow$ A4) between OH–isoprene adducts are hindered due to very high activation energies (Figure 10.3) [70]. The calculated rate constant is in agreement with the experimental values [69,73–77], confirming the accuracy of the selected levels of theory. Kinetic calculations employing RRKM/ME method show a consistence of fall-off behavior for OH–isoprene reaction with the recent experimental measurements at low pressure [70]. The branching ratio at the low-pressure limit was predicted by Stevens [75], with values of 0.72 and 0.28 for isomer A1 and A4, respectively, and less than 1% for both isomer A2 and A3. The β-hydroxyl alkyl radical from internal addition of OH has been suggested to undergo cyclization to produce α-hydroxy radical [78] and result in the formation of C5 carbonyls, whose yields have been estimated recently [68]. While Lei *et al.* [70,72] found that addition of OH to isoprene proceeds without an activation barrier, Francisoco-Marquez *et al.* [79] using both density functional theory and Moller–Plesset perturbation theory to the second-order (MP2) showed the formation of pre-reactive complexes and large activation energies for the internal carbon addition. They concluded that the internal addition pathways are unlikely responsible for the formation of 3-methyl furan; the likely pathways for the formation 3-methyl furan are via external addition according to their recent theoretical calculations [80]. Francisoco-Marquez *et al.* [80] also predicted negative activation energies for addition at the terminal carbon atoms for the OH–isoprene reaction. In general, activation energies obtained using DFT are rather unreliable.

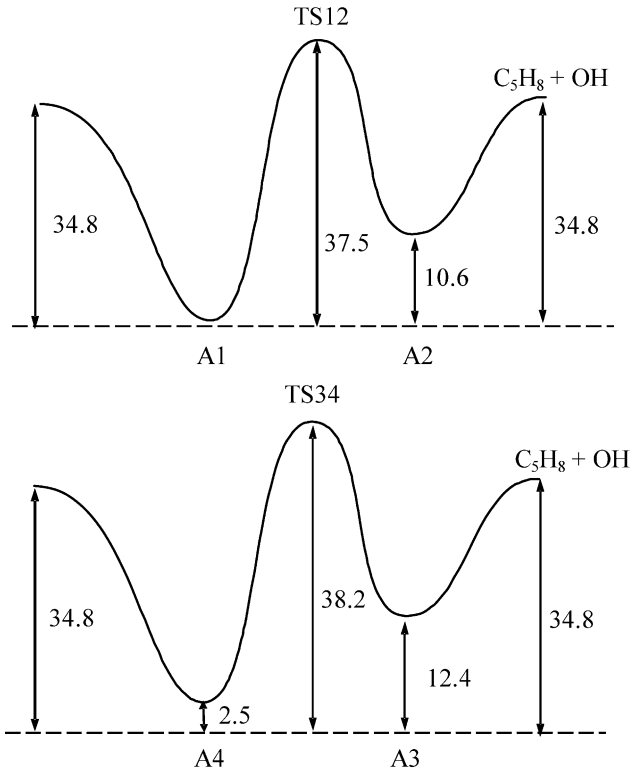

FIGURE 10.3 Schematic potential energy surfaces for the inter-conversions of OH–isoprene adduct reactions calculated at the CCSD(T)/6-311G(d,p)//B3LYP/6-31G(d,p) level of theory.

Peroxy radicals involve in many reactions as key intermediates in propagating catalytic cycles, which lead to ozone formation in the troposphere. The reactivity of the peroxy radicals depends strongly on the structure of the radicals. The geometries of six isoprene peroxy radical isomers (without Z-configuration isomers) are obtained and the peroxy radicals are more stable than the separated reactants (isoprene, OH and O_2) by 47–53 kcal mol^{-1} at CCSD(T)/6-31G(d) level of theory [81]. The CVTST calculations predict branching ratios of 0.60:0.40 for isomer A and B and 0.78:0.22 for isomer F and G [81]. The strong propensity for isomers A, B and F is predicted in good agreement with the model of Jenkin and Hayman [82], but qualitatively different from the model of Paulson and Seinfeld [83]. Jenkin and Hayman suggested the branching ratios based on the assumption that the peroxy radical center would form at the more substituted site. The predicted high-pressure limit rate constants are significantly faster than the corresponding rates associated with O_2 addition to aromatic–OH adducts, but slower than the reaction of O_2 with alkyl and hydroxyalkyl radicals. It is speculated that the calculated branching ratios and rate constants of the peroxy radicals are mostly dependent on their binding energies and the nature of the transition states, not on their relative stability. Peroxy radicals have been detected and a rate constant

of 7×10^{-13} cm^3 molecule^{-1} s^{-1} for the reaction of OH–isoprene adducts with O_2 has been determined from the decay of the peroxy radicals detected by the chemical ionization mass spectrometry (CIMS) [84], while Park *et al.* [85] reported a rate constant of 2×10^{-12} cm^3 molecule^{-1} s^{-1} for the same reactions using laser photolysis/laser-induced fluorescence technique.

The reaction of hydroxy peroxy radicals (RO_2) with NO represents one of the most crucial tropospheric processes, leading to terrestrial ozone formation or NO_x removal and chain termination. The C–C bond fission of the resultant OH–isoprene alkoxy radicals was investigated by Dibble [65]. It is found that the low barrier heights (0.7–2.1 kcal mol^{-1} at B3LYP/6-311G(2df, 2p) level) for the decomposition of four β-hydroxyalkoxy radicals allow this channel to be dominant, while in contrast decomposition of δ-hydroxyalkoxy radicals possesses high barrier heights and endothermic characteristics (16–20 kcal mol^{-1}), rendering this pathway unimportant in the atmosphere. The results from theoretical calculations provide useful information to assess the potential detection of these alkoxy radicals in the laboratory based on the stabilities and it has been pointed out that the β-hydroxyalkoxy radical is difficult to be probed due to their short lifetime (picoseconds). Lei and Zhang [66] carried out higher levels of *ab initio* calculations to investigate the geometries and energetics of the alkoxy radicals and their decomposition pathways. They found that activation energies for the preferable decomposition pathway fall in the range of 6–7 kcal mol^{-1} for the β-hydroxyalkoxy isomers and 18–21 kcal mol^{-1} for δ-hydroxyalkoxy isomers, providing more accurate and reliable activation energies. The activation barriers for decomposition of alkoxy radicals calculated by Dibble are lower than those calculated by Lei *et al.*, and the difference between the two studies is explained since the B3LYP level of theory is notorious for under-prediction of barrier height. Thermal decomposition of hydroxylalkoxy I and IV is mainly responsible for the formation of the major isoprene-OH products: methyl vinyl ketone (MVK) and methacrolein (MACR) (Figure 10.4) [66]. Ramirez-Ramirez *et al.* [86] investigated the formation and interconversion of cis- and trans-isomer of the MVK from the alkoxy radical I at MP2/6-31G(d)//B3LYP/6-31G(d,p) level and found that the barrier heights are comparable to the ones reported by Lei and Zhang [66] at the similar level. Park *et al.* performed kinetic calculations using RRKM/ME method to investigate the temperature and pressure dependent rate constants between 220 and 310 K and found similar features in the fall-off region for the β-hydroxyalkoxy radicals [87]. The high-pressure limit rate constants for the β-hydroxyalkoxy radicals obtained from RRKM/ME calculations are close to the values from TST calculations [66]. The rapid decomposition of the energized β-hydroxyalkoxy radicals may play an important role in the overall decomposition pathways since significant fraction of them (except for isomer I) was found to undergo prompt reactions. However, a rate constant of 3×10^4 s^{-1} was reported using laser photolysis/laser-induced fluorescence technique [88], which is significant lower than those values from Lei and Zhang [66] and Dibble [65], in the range of 10^8–10^{10} s^{-1}. A rate constant of 9×10^{-12} cm^3 molecule^{-1} s^{-1} for reactions of the peroxy radicals with NO was reported from the decay of the peroxy radicals using the CIMS detection [84], which is consistent with the predicted rate constant using the CVTST [66]. A higher

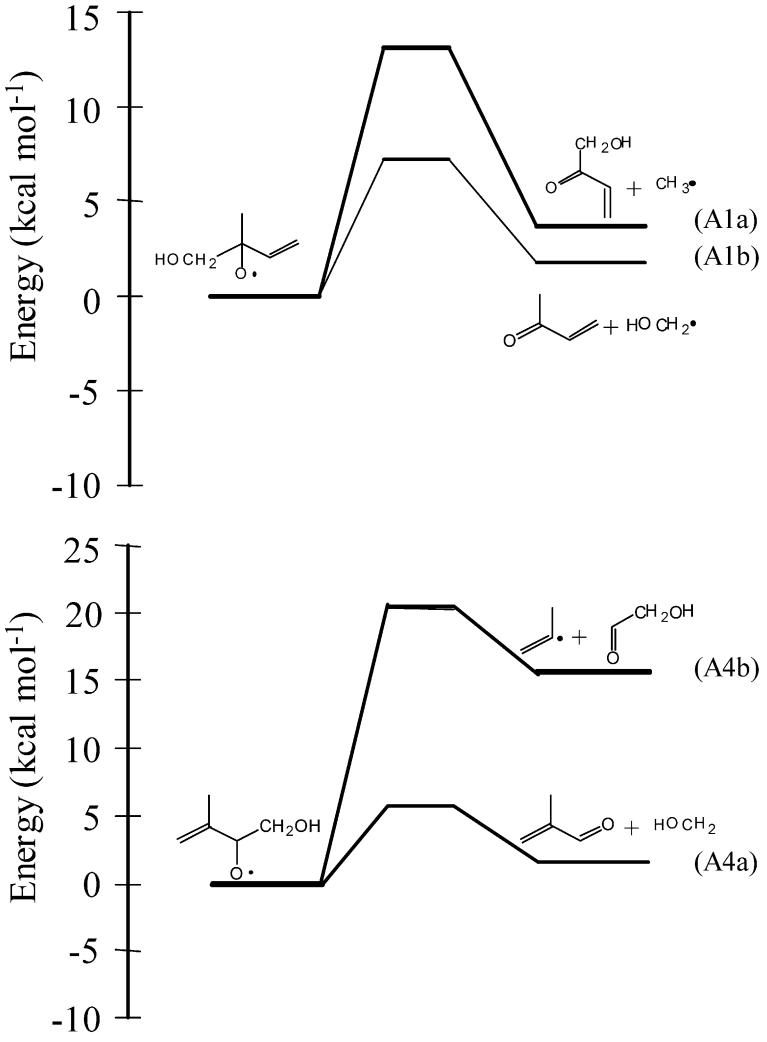

FIGURE 10.4 Potential energy surfaces for the C–C bond fission of radicals I and IV obtained at the CCSD(T)/6-31G(d) + CF//B3LYP/6-31G(d,f) level of theory.

value of 2.5×10^{-11} cm^3 molecule^{-1} s^{-1} was obtained using laser photolysis/laser-induced fluorescence technique [88]. For the β-hydroxy-peroxy radicals with an unsaturated C=C bond, addition of one more oxygen molecule leads to unimolecular ring-closure (Figure 10.5) (forming a bridge between the oxygen of radical center and the unsaturated terminal carbon), forming a 6-membered ring structure radicals (cycloperoxide-peroxy radicals) with high oxygenated content, which potentially alter the final product distribution of the OH–isoprene system and have important implication for secondary organic aerosol (SOA) formation. For example, Vereecken and Peeters presented a theoretical study of such reactions and

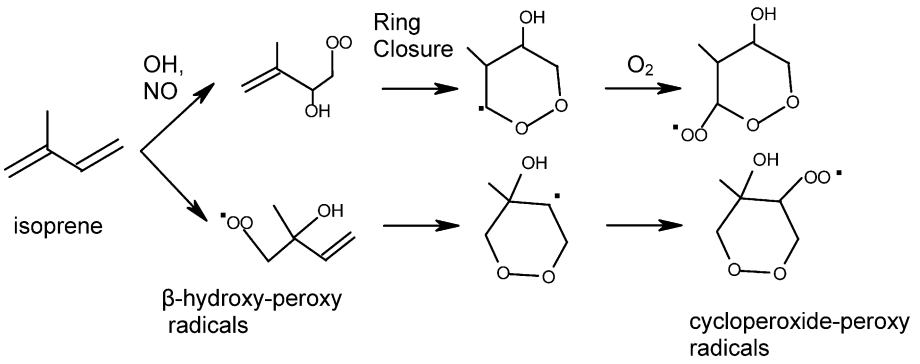

FIGURE 10.5 Mechanistic representation of the ring-closure reactions for the β-hydroxy-peroxy radicals arising from the OH–isoprene reactions.

found that in low NO_x or even moderately polluted atmosphere (e.g., 1 ppbv NO) the rates of ring closure dominate or are comparable to the reaction with NO [89].

The reactions of hydroxy peroxy radicals (RO_2) with NO lead to major formation of alkoxy radicals and minor production of organic nitrates. It has been proposed that these two channels are bridged via a common hydroxy peroxy nitrite intermediate. Similar to the scheme in Figure 10.1, the entrance channel of the RO_2–NO reaction is exoergic by about 20 kcal mol^{-1}, leading to a vibrationally excited hydroxyperoxy nitrite (ROONO*), which subsequently reacts via unimolecular reactions or collisional stabilization [51]. The excited or thermalized nitrite undergoes two possible prompt unimolecular reactions, isomerization to the isoprene nitrate ($RONO_2$) or decomposition to a hydroxyalkoxy radical (RO) and NO_2. The high-pressure limit rate constants for the formation of the ROONO isomers at 300 K were calculated using CVTST method, with values of $3–10 \times 10^{-12}$ cm^3 molecule^{-1} s^{-1} [51], consistent with the two experimental results mentioned above (9×10^{-12} and 2.5×10^{-11} cm^3 molecule^{-1} s^{-1}) [84,88]. The fate of the excited hydroxyperoxy nitrites was assessed using the steady-state master equation (ME) formalism in conjunction with the variational-RRKM (vRRKM/ME) method [51]. The entrance channel and the exit channel (dissociation of the nitrite to RO and NO_2) were found to be barrierless according to the quantum chemical calculations because the calculated energy relative to the equilibrium peroxynitrite increased monotonically when the O–O bond length was successively increased at the B3LYP/6-31G(d,p) level. The results indicated that at all energies above the entrance channel (20.2 kcal mol^{-1}) the dissociation rates are larger than the collision rate and the formation of thermalized nitrite is insignificant under ambient conditions. On average, loss of the nitrite internal energy due to collisions is insignificant (1–4 kcal mol^{-1}).

Rearrangement of the peroxynitrite to nitrate has been a long outstanding issue. A previous theoretical study suggested that this rearrangement proceeds via a three-centered transition state, which for HOONO corresponds to an activation energy of about 60 kcal mol^{-1} [89–92]. However, the three-centered transition state is likely hindered by the substitute of a carbon chain to the hydrogen atom, and

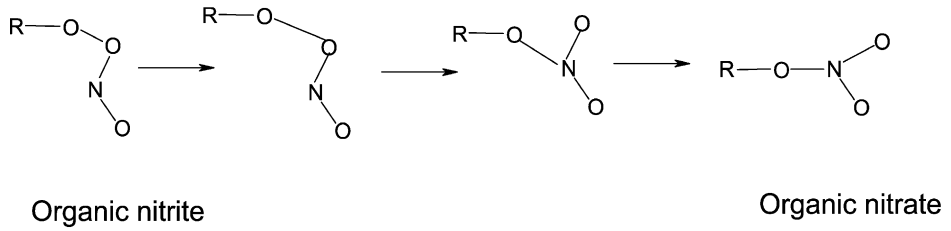

FIGURE 10.6 Schematic representation of isomerization of organic nitrite to nitrate.

the rearrangement of ROONO to $RONO_2$ may go through a partial O–O bond fission followed by RO and NO_2 recombination at elongated O–O bond lengths (Figure 10.6). Several experimental studies have reported the nitrate yield from the OH-initiated oxidation of isoprene, ranging from 4 to 12% [93]. Using the vRRKM/ME analysis and the experimentally determined nitrate yield, Zhang *et al.* [51] predicted that the activation barrier of ROONO isomerization to $RONO_2$ is between 0.4 and 1.1 kcal mol^{-1} below and 3.3–3.7 kcal mol^{-1} above the dissociation energy of ROONO, significantly lower than the barrier height for the three-center transition state in HOONO [89–92].

For both thermalized and activated β-hydroxyalkoxy radicals, the dominant fate is decomposition, leading to the formation of various oxygenated organic compounds. For the δ-hydroxyalkoxy radicals, however, the decomposition channel is minor due to the high barrier height, and other channels (e.g., H-abstraction and H-migration) are more important. Zhao *et al.* [94] investigated the competing pathways of H-abstraction by oxygen molecules and 1,5 H-shift of the δ-alkoxy using multiple level calculations (B3LYP, CCSD(T), and MPW1K with various basis sets) to obtain the geometries and energetic information of these two reactions. The B3LYP significantly underestimates the activation barriers, while the CCSD(T) and MPW1K give comparable results in predicting the activation barriers. Kinetic calculations employing vRRKM/ME formalism and separate statistical ensemble (SSE) theory showed that a significant fraction of the chemically excited alkoxy radicals undergo prompt 1,5 H-shift. The results revealed that 1,5 H-shift of thermalized δ-alkoxy radicals dominates over H-abstraction by O_2 (see Figure 10.7). The consecutive reactions of the dihydroxy radical intermediates with O_2 form hydroxycarbonyls which have been qualitatively observed [95,96] and quantified [68], with a yield of about 19%. Ramirez-Ramirez *et al.* [97] performed *ab initio* calculations of subsequent reactions of the dihydroxyl radicals and found that these reactions occur quickly in atmospheric conditions and proceed without an energy barrier, providing an explanation for the observed formation of hydroxylcarbonyls. Alternatively, the resonant allylic dihydroxyl radicals can form dihydroxyperoxy radicals by O_2 addition and subsequently react with NO to produce the corresponding alkoxy radicals [98]. These second-generation of peroxy and alkoxy radicals exhibit two intramolecular hydrogen bonds and the simultaneous transfer of two H-atoms across the hydrogen bonds with a barrier of only about 5 kcal mol^{-1} in the alkoxy radicals, but about 20 kcal mol^{-1} in the peroxy radicals. These double H transfer reactions in the alkoxy radicals are exother-

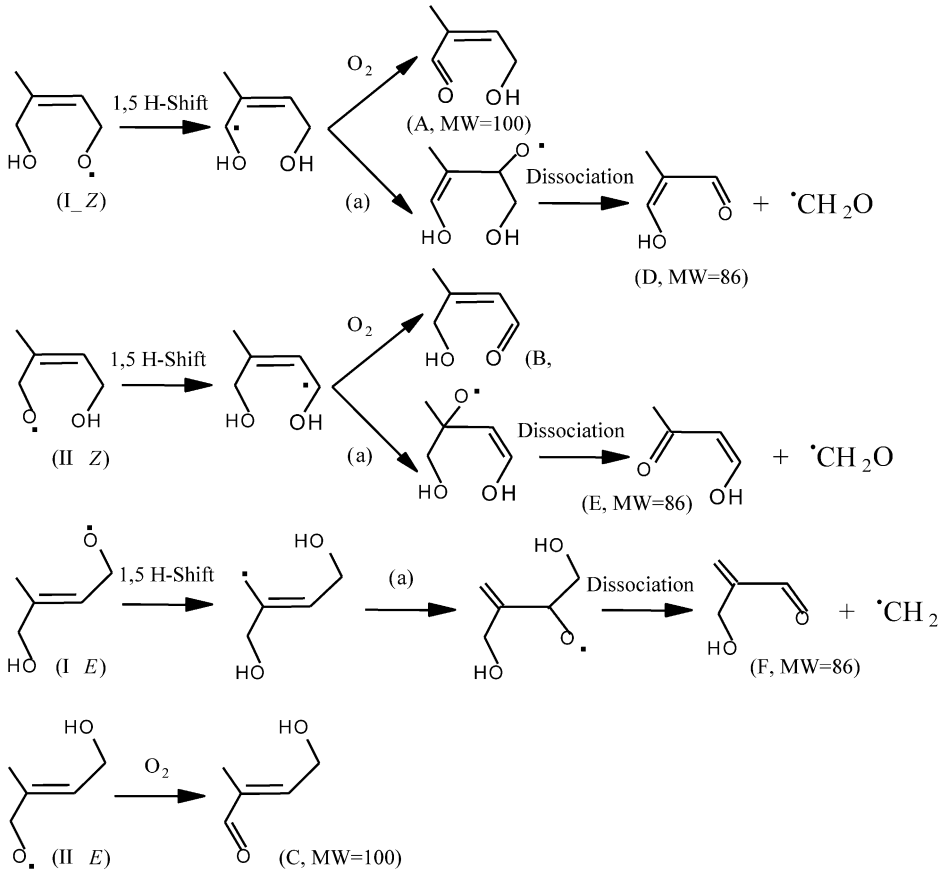

FIGURE 10.7 Reaction mechanisms of the δ-alkoxy radicals arising from the OH–isoprene reactions.

mic and their fates are governed by competition between collisional stabilization and prompt decomposition. The thermalized alkoxy radicals are further decomposed to form C4-hydroxycarbonyls, which has been detected and quantified recently [68].

3.1.2 O_3-initiated oxidation

While reaction with OH is the dominant tropospheric removal pathway for isoprene, a substantial amount of isoprene is also degraded by reaction with ozone in the troposphere. There exists increasing evidence that the OH radicals are formed during the course of ozonolysis of isoprene, providing an important source of nighttime OH radicals on the regional scale [99]. Ozonolysis of isoprene may also play an important role in SOA formation since low volatile organic compounds generated from this process are potential precursors of SOA [100,101]. The initial ozonolysis reaction occurs primarily by cycloaddition of O_3 to either one of the >C=C< double bonds of isoprene, resulting in the formation of primary ozonide

(POZ). The reaction enthalpy is retained as the internal energy of the products, resulting in formation of the vibrationally excited ozonide, which subsequently undergoes unimolecular decomposition to yield a chemically activated biradical, known as the carbonyl oxide or Criegee intermediate (CI), and an aldehyde (e.g., MVK, MACR or formaldehyde). A total of nine carbonyl oxides (methyl vinyl carbonyl oxide, derived from 1,2-ozonide; isopropyl carbonyloxide, derived from 3,4-ozonide and formaldehyde oxide, H_2COO from both ozonide) are formed and a large fraction of these carbonyl oxides with ample internal energy facilitates prompt unimolecular reactions or stabilization. Two primary reaction pathways exist for the vibrationally excited carbonyl oxide, ring closure to form dioxirane or H-migration to form a hydroperoxide intermediate. There are several pathways leading to the formation of OH radicals: (1) the resulting hydroperoxide decomposes to form OH and RCO radicals; (2) decomposition of dioxirane may lead to formation of vibrationally excited organic acids which may also dissociate to form OH; and (3) the cleavage of the O–O bond in the primary ozonides results in formation of OH radicals via an unstable hydroperoxide intermediate. Figure 10.8 [69] summarizes the mechanistic diagram of the ozonolysis of isoprene, which only consider the major reaction pathways. The OH formation yield has been measured experimentally by several methods (e.g., indirect scavenger method and direct laser-induced fluorescence detection) with values in a wide range of 0.19–0.53 [102–106]. Theoretical investigation of isoprene ozonolysis fo-

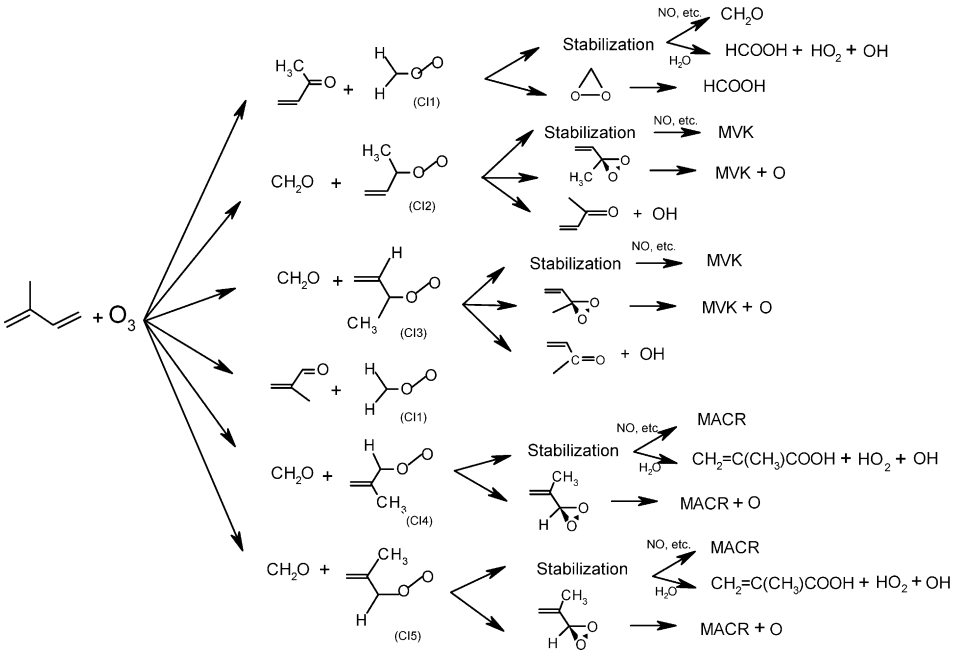

FIGURE 10.8 Mechanistic diagram of ozonolysis of isoprene.

cuses on the formation of OH radicals and the subsequent reactions of the carbonyl oxides.

The reaction of ozone with isoprene involves a series of reactions and intermediates, with excessive reaction energy propagating among the intermediates and products. The reaction mechanism of ozone with isoprene is not as well understood as that of OH with isoprene in both experimental and theoretical aspects. In addition, since the lifetimes of most of the intermediates are very short, experimental detection of these intermediate species is extremely difficult. Hence, theoretical methods provide an alternative tool to investigate the formation of the intermediates and their fates in the ozone–isoprene system. Gutbrod *et al.* [107] performed both experimental and theoretical investigation of the formation of various syn and anti stereoisomers of the carbonyl oxides from ozonolysis of isoprene and reported their structures and energies at the B3LYP/6-31G(d,p) level of theory. An OH formation yield of 19% was obtained and the OH radicals were primarily from the decomposition of carbonyl oxides depending on a syn-positioned methyl (alkyl) group and the interaction with the terminal O atom of a carbonyl oxide. Quantum chemical calculations showed that the formation of hydroperoxide is more favorable than isomerization to dioxirane for carbonyl oxides, with a barrier of 15.5 verse 23 kcal mol^{-1} for the two channels at level of CCSD(T)/6-31G(d,p)//B3LYP/6-31G(d,p), respectively. Zhang and Zhang [108] performed density functional theory and *ab initio* calculations to investigate the formation and unimolecular reactions of primary ozonides and carbonyl oxides from isoprene ozonolysis and found no significantly preferential branching for the initial step of O_3 cycloaddition to the two double bonds of isoprene. Cleavage of thermalized primary ozonides to form carbonyl oxides occurs with barriers of 11–16 kcal mol^{-1} above the ground state of the primary ozonides. However, the collisional stabilizations of the primary ozonides are negligible under atmospheric conditions. Prompt dissociation of the excited primary ozonides leading to formation of syn and anti conformations of carbonyl oxides should be considered due to the large exothermicity associated with the formation of the primary ozonides. The OH formation is shown to occur primarily via decomposition of the carbonyl oxides with the syn-positioned methyl (alkyl) group, which is more favorable than isomerization to form dioxirane (by 1.1–3.3 kcal mol^{-1}). An OH formation yield of 0.25 from prompt and thermal decomposition of the carbonyl oxides was estimated using the transition state theory and master equation formalism. A calculated rate constant of 1.58×10^{-17} cm^3 $molecule^{-1}$ s^{-1} for the O_3-isoprene is in agreement with the experimental value (1.4×10^{-17} cm^3 $molecule^{-1}$ s^{-1}). In another study, Zhang *et al.* [109] evaluated the fate of primary ozonides and carbonyl oxides using a statistical–dynamical master equation and transition state theory and the results showed that excited carbonyl oxides promptly dissociate to produce OH (11%) or isomerize to form dioxirane (32%), while the remaining (57%) are collisionally stabilized. An OH formation yield of 0.25 obtained from previous study [108] was distributed to prompt (0.11) and thermal (0.14) decomposition of the carbonyl oxides. The results reveal slow thermal decomposition of the carbonyl oxide to form OH due to high activation barriers. Except for OH radicals, the yields of the stable products formaldehyde, MACR, and MVK are estimated to be 0.67, 0.21, and 0.12,

respectively. A very recent study by Kuwata *et al.* [110] provided a new insight into the isoprene ozonolysis using CBS-QB3 calculations and RRKM/master equation simulations. Kuwata *et al.* investigate the formation of the methyl vinyl carbonyl oxides and the interconversion among four possible conformers, and their isomerization. They predicted an OH formation yield of 19%, quantitatively consistent with the experiment value assuming that all thermalized syn-methyl carbonyl oxides form OH. A predicted MVK formation yield of 0.17 is in agreement with the current recommended experimental MVK yield of 0.16 [110–112]. Natural bond order (NBO) analysis reveals that the effect of the vinyl group has profound impact on the chemistry of the methyl vinyl carbonyl oxide by lowering the barrier to rotation about the C=O bond and allowing the carbonyl oxide to cyclize to form a dioxole [110], which was not considered previously. Dioxole formation with an activation barrier of 13.9 kcal mol^{-1} at CBS-QB3 level is predicted to be favored over other channels (e.g., vinyl hydroperoxide formation, dioxirane formation, and collisional stabilization). Kuwata *et al.* [110] also concluded that two dioxole derivatives, 1,2-epoxy-3-butanone and 3-oxobutanal, are major products of isoprene ozonolysis, which need to be investigated experimentally in the future study. Hence, there still exists discrepancy among the above studies: it needs to be verified that the complete basis set (CBS) employed in Kuwata *et al.* provide more accurate prediction of the branching ratios and hence the OH yield than those in the two previous studies.

An important fraction of carbonyl oxides are collisionally stabilized and further react with other atmospheric species (e.g., water, sulfuric dioxide and sulfuric acid [113]). The reaction with water vapor represents one of the most important processes for the atmospheric degradation of the stabilized carbonyl oxides and is known to lead to the formation of α-hydroxy hydroperoxide compounds, organic acids, aldehydes, and H_2O_2 [114–118]. Figure 10.9 shows the schematic mechanisms for the reactions between carbonyl oxides and water. Two reaction pathways have been proposed: (1) An α-hydroxy hydroperoxide is formed by addition of the water molecule to the carbonyl oxide; (2) Water-assisted hydrogen migration occurs to the terminal oxygen of the COO group and subsequent OO bond cleavage lead to the formation OH radicals. Aplincourt and Anglada [119] presented a

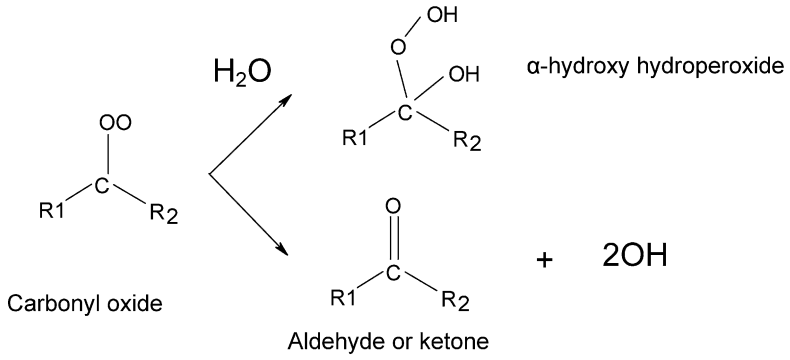

FIGURE 10.9 Schematic representation of reactions of carbonyl oxides with water.

theoretical investigation of the stabilized isoprene carbonyl oxides with water and found formation of a stable hydrogen-bond complex (about 6 kcal mol^{-1} more stable than the reactants). The water addition involve in a five-membered ring transition state and is the most favorable reaction channel with the activation enthalpies of about 14 kcal mol^{-1} and 9 kcal mol^{-1} at G2M-RCC5//B3LYP/6-311 + G(2d,2p) level (a modified Gaussian 2 theory) of theory for carbonyl oxides derived from 1,2- and 3,4-ozonide, respectively. The water-assisted hydrogen migration path corresponds to the water catalyzed reaction of the unimolecular decomposition pathway involving in a seven-membered ring transition state and is a possible source of atmospheric OH radicals. Furthermore, the water-catalyzed effect reduces the activation enthalpy by ~7 kcal mol^{-1} (at CCSD(T)/6-31G(d) + CF level) compared to the decomposition pathways reported by Zhang and Zhang [108]. However, the resultant activation barriers are still higher than those of the water addition reaction, rendering this pathway unimportant compared to the water addition reaction. Kinetic calculations employing transition state theory showed that only two water-catalyzed reaction channels involving the hydrogen transfer from the β-hydrogen (with respect to the COO group) in syn position to the terminal oxygen of the COO group are accessible with a branching ratio of 13–20% at temperature 273–298 K. Another theoretical study by Aplincourt and Anglada [120] showed that the unimolecular decomposition of both α-hydroxy hydroperoxides requires very high activation enthalpies (~44 kcal mol^{-1}), rendering this pathway implausible in the atmosphere. On the other hand, lower activation enthalpies have been found for the water-assisted decomposition of these α-hydroxy hydroperoxides. The reaction between α-hydroxy hydroperoxides derived from 1,2-ozonide and H_2O leads to the formation of MVK and H_2O_2 exclusively. The reaction between α-hydroxy hydroperoxides derived from 3,4-ozonide and H_2O has two possible reaction channels, MACR+H_2O_2 and methacrylic acid (MTA)+H_2O, respectively. However, the activation enthalpies and the computed unimolecular reaction constants reveal that the reaction is almost exclusively MACR + H_2O_2. Ryzhkov and Parisa [121,122] presented theoretical studies of the reactions of carbonyl oxides with water and its clusters. They found that the most kinetically favorable pathway is the reaction with water dimer, which involves a seven-member ring transition state. The authors also found that the relative humidity may influence the rates and reaction mechanisms. For example, the rate constants of the carbonyl oxides and water clusters are increasing with relative humidity. The results indicate that the reaction mechanisms may be different under different humidities.

3.1.3 NO_3-initiated oxidation

The nitrate radical, formed by the reaction of NO_2 and ozone, is a major tropospheric nighttime oxidant and its mixing ratio can reach up to several hundred ppt at night [123]. The nighttime reaction between isoprene and nitrate radical contributes significantly to the degradation of isoprene [124,125]. The reaction between isoprene and NO_3 occurs by NO_3 addition to the >C=C< bonds, forming thermodynamically favored nitrooxyalkyl radicals. Under atmospheric conditions, the nitrooxyalkyl radicals react primarily with oxygen molecules to form

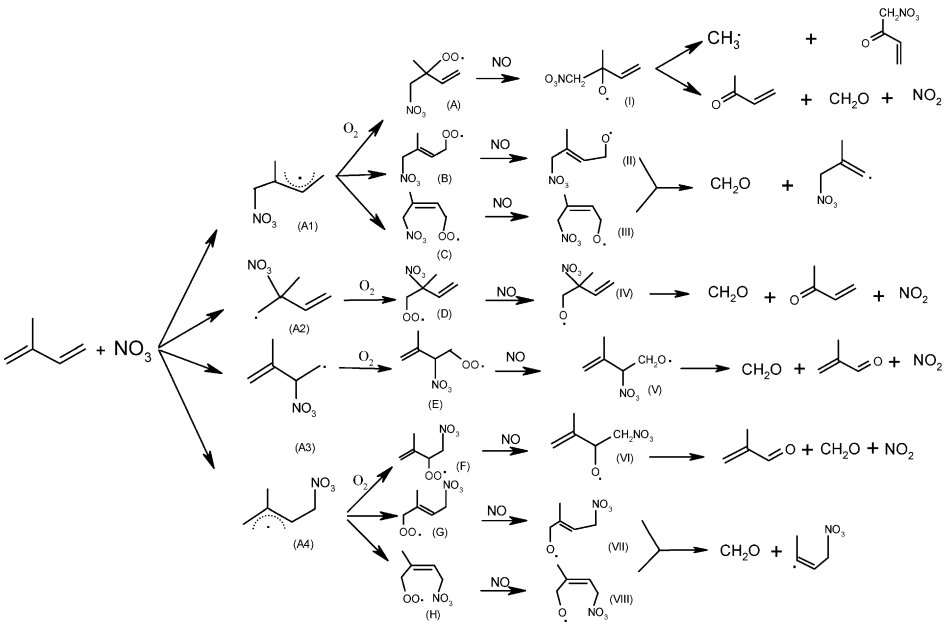

FIGURE 10.10 Mechanistic diagram of NO_3-initiated oxidation of isoprene.

nitrooxyalkyl peroxy radicals. Similarly to the OH–isoprene reaction, addition of O_2 occurs only at the carbons β to the NO_3 position for the NO_3–isoprene adducts of internal NO_3 (C2- and C3-position) addition, but takes place at two centers (β or δ to the NO_3 position) for terminal NO_3 (C1- and C4-position) addition, leading to the formation of β- and δ-nitrooxyalkyl peroxy radicals. The δ-nitrooxyperoxy isomers include both *E* and *Z* configurations. The nitrooxyalkyl peroxy radicals can further react with NO or engage in a self-reaction or cross-reaction with other peroxy radicals to form nitrooxyalkoxy radicals, or react with HO_2 to form nitrooxyperoxide. The nitrooxyalkoxy radicals can undergo isomerization or decomposition, or abstraction by O_2, leading to various oxygenated or nitrated organic species. Figure 10.10 represents the mechanistic diagram of the NO_3-initiated oxidation of isoprene. Current, only a few theoretical studies have been reported in the literature on the NO_3 initiated isoprene oxidation. Suh *et al.* [126] reported the structures and energies of the NO_3–isoprene adduct isomers employing density functional theory and *ab initio* calculations and the rate constants of the formation of the NO_3–isoprene adducts and their isomeric branching have been calculated using the canonical variational transition state theory. The calculated isomeric branching suggested preferential addition of NO_3 to C1 position (a ratio of 0.84), consistent with previous product studies of the NO_3–isoprene reaction system [127,128]. Zhang and Zhang [129] investigated unimolecular decomposition of nitrooxyalkyl radicals from NO_3–isoprene reaction using quantum chemical calculations, CVTST, and master equation analysis. The results indicated that the channel leading to the formation of the two oxiranes proposed by Berndt

and Boge [128] is negligible. Instead, the chemically activated nitrooxyalkyl radicals become stabilized by collision and the thermal nitrooxyalkyl radicals mainly react with O_2 to form the nitrooxyalkyl peroxy radicals, which contribute to the formation of MACR and MVK. Zhao and Zhang [130] presented the structures and energetics of the eight peroxy radicals arising from NO_3–isoprene reactions using density functional theory and *ab initio* methods and the rate constants for addition of O_2 to the NO_3–isoprene adducts using CVTST. The results provided the isomeric branching ratios between the NO_3–O_2–isoprene peroxy radicals and predicted a ratio of 7.4 of 1,2-addition to 4,3-addition, in agreement with the experimental value reported by Berndt and Boge [128], almost two fold higher than the experimental values by Skov *et al.* [127]. No explanation was given for the discrepancy between the two experimental results. Zhao and Zhang [131] also investigated the structures and energetics of the alkoxy radicals and their decomposition pathways. For both thermalized and activated β-alkoxy radicals the dominant fate is decomposition, but for δ-hydroxy alkoxy radicals the decomposition channel is minor due to a large barrier and the H-abstraction and H-migration channels are more important, similar to the alkoxy radicals of OH–isoprene systems.

3.1.4 Cl-initiated oxidation

The reaction between isoprene and chlorine atoms may play an important role both in the continental troposphere and in the marine boundary layer [132–135]. The initial reaction between isoprene and Cl is believed to proceed mainly by Cl addition to the C=C bond, forming a Cl–isoprene adduct radical. Alternatively, Cl can abstract one hydrogen atom from methyl group of isoprene to form HCl and an allylic radical. Under the tropospheric conditions, the adduct reacts primarily with oxygen molecules to form the β-chloroalkenylperoxy radicals. In the presence of nitric oxide NO, initial Cl radical addition at the C1-, C2-, C3-, or C4-positions with subsequent addition of O_2 at the C2-, C1-, C4-, and C3-positions, respectively, leads to the formation of β-chloroalkenylalkoxy radicals. The dominant tropospheric reaction of β-chloroalkenylalkoxy radicals is unimolecular decomposition or bimolecular reaction with oxygen molecule, leading to the formation of various oxygenated and nitrated organic compounds (Figure 10.11). A rate constant of $(3.4–4.6) \times 10^{-10}$ cm^3 molecule^{-1} s^{-1} has been determined experimentally for the reaction between Cl and isoprene [136–140] and the branching ratio for the initial addition and abstraction reaction has been inferred from the HCl formation yield, with values between 13% and 17% [136,137]. Various final products have been identified including CO, CO_2, formyl chloride, formic acid, methylglyoxal, hydrogen chloride, and 1-chloro-3-methyl-3-buten-2-one (CMBO, a tracer for chlorine radicals) [136,137]. However, direct experimental data concerning intermediate processes of the oxidation reactions of isoprene with Cl are very limited, due to the lack of sensitive detection schemes for these species. Lei and Zhang [141] reported the first quantum chemical calculations on the Cl–isoprene oxidation and found the isomers with Cl addition to the terminal C1-position are the most energetically favorable. The activation energies for interconversion between isomers are low ($\sim$2.8–4.7 kcal mol^{-1}), indicating that thermal equilibrium between the isomers is easily established. The formation rates and isomeric branching ratios were

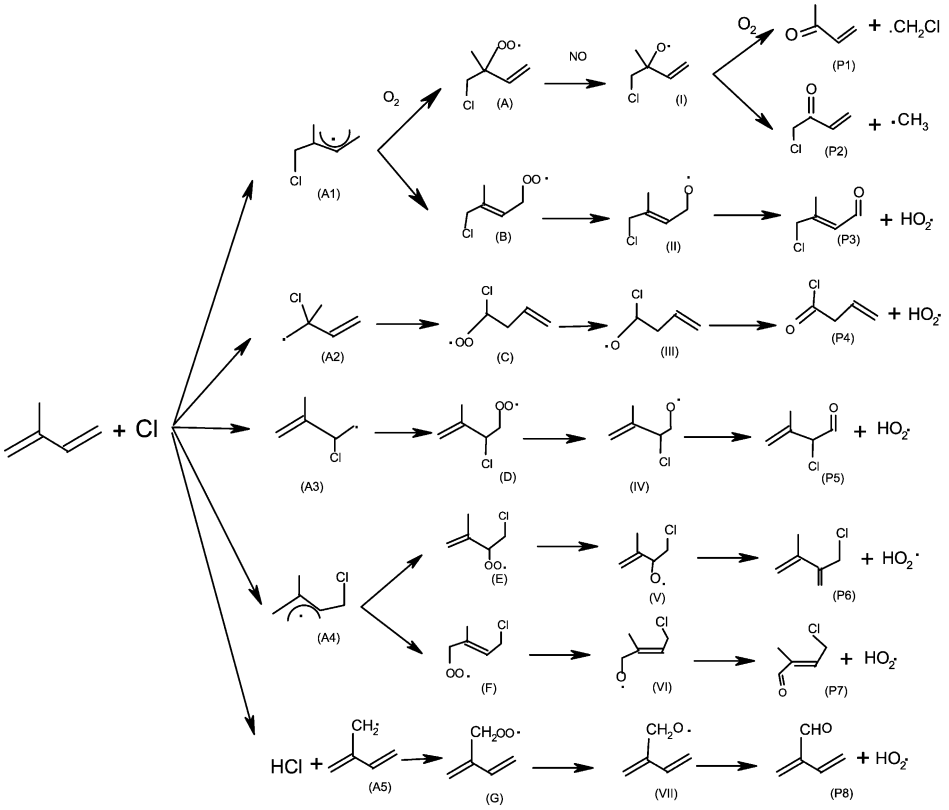

FIGURE 10.11 Mechanistic diagram of Cl-initiated oxidation of isoprene.

calculated using CVTST [142]: a rate constant of 4.2×10^{-10} $cm^3\,molecule^{-1}\,s^{-1}$ is determined and a strong preference is found for Cl addition to the terminal carbon, with an amount of ~90% for the terminal addition. RRKM/ME calculations show that almost all of the adducts from the terminal addition are collision stabilized, while adducts from internal addition undergo exclusively prompt isomerization and the collisional stabilization can be negligible under atmospheric conditions. No activation barrier is found for Cl addition to isoprene and the Morse potential well represents the energetics along the reaction coordinate. Brana and Sordo [143] investigated the abstraction channel and found that the reaction proceeds through an association-elimination mechanism in which a weakly bound intermediate is formed via a six-membered ring transition state, followed by HCl elimination leading to the final the allylic radical formation. DFT and *ab initio* molecular orbital calculations have been performed to investigate the structures and energetics of the Cl–O_2–isoprene peroxy radicals: the peroxy radicals are ~39 to 43 kcal mol^{-1} more stable than the separated reactants at the CCSD(T)/6-31G(d) level of theory [144]. The O_2 addition is found to be barrierless and the rate constants are calculated using CVTST based on the Morse potential to describe the

reaction coordinate, in agreement with the experimental values [145]. The results indicate that the two β-chloroalkenylperoxy radicals with initial Cl addition at C1 and C4 positions and subsequent O_2 addition at C2 and C3 positions, respectively, play an important role in determining the reaction pathways and final product distributions of the Cl–isoprene reaction system. The predicted branching ratio facilitates the application of CMBO as a tracer to deduce chlorine radical concentrations in the urban and regional atmosphere. Density-functional theory and *ab initio* calculations have been employed to explore the structures and energetics of the chloroalkenyl alkoxy radicals and their decomposition pathways [146]. The activation and reaction energies of C–C bond scission of the alkoxy radicals are in the ranges of 12–25 and 23–22 kcal mol^{-1}, respectively. The results indicate that C–C bond decomposition of the chloroalkenyl alkoxy radicals is rather slow and likely plays a minor role in the Cl–isoprene reactions, consistent with laboratory studies which show small MVK and MACR yields but significant CMBO formation. A yield of 30% is predicted for CMBO formation from Cl-initiated oxidation of isoprene. Considering the potential importance of the Cl–isoprene reactions, more studies of Cl-initiated isoprene oxidation are needed to assess the product distribution of the Cl–isoprene reactions in the future.

Recently, the explicit oxidation mechanism of isoprene initiated by OH, O_3, NO_3, and Cl, incorporating the most recent laboratory and theoretical studies, has been evaluated using a box model [69]. The updated mechanism provides explicit reaction steps and detailed intermediates for isoprene oxidation and facilitates more accurate modeling of isoprene photochemistry in the atmosphere.

3.2 Pinenes

Monoterpenes account for ~10% of the total biogenic hydrocarbons globally, with α- and β-pinene being the most abundant monoterpenes emitted in North America [1]. The pinenes (α- and β-pinene) are removed from the atmosphere primarily by reactions with OH radicals, NO_3 radicals and O_3 [12]. Due to their high reactivity toward oxidants, atmospheric oxidation of the pinenes contributes significantly to ozone and SOA formation in the troposphere. The OH reactions dominate during daytime while reactions with NO_3 and O_3 are significant at night. The OH reactions proceed mainly by initial addition to the endocyclic (for α-pinene) or exocyclic (for β-pinene) C=C double bond, resulting in the formation of β-hydroxylalkyl radicals. Subsequent reaction of β-hydroxylalkyl radicals with other atmospheric constituents (e.g., O_2 and NO) or isomerization leads to multifunctional products (e.g., aldehydes, ketones and carboxylic acids) in both gas phase and particulate phase. Alternatively, H-abstraction can account for ~10–20% of the total reaction rate, forming allyl resonance stabilized α-pinenyl radicals. Figure 10.12 shows an overview of the OH-initiated oxidation of α-pinene.

The initial step of the OH–pinenes reaction has been investigated using density functional theory and *ab initio* methods by Fan *et al.* [147] (for α- and β-pinenes) and Ramirez-Ramirez *et al.* [148] (for β-pinene). Both studies considered site-specific and stereo-specific (anti and syn position relative to the $-C(CH_3)_2-$ bridge) addition of OH to the pinene C=C bond, forming four adducts for each pinene.

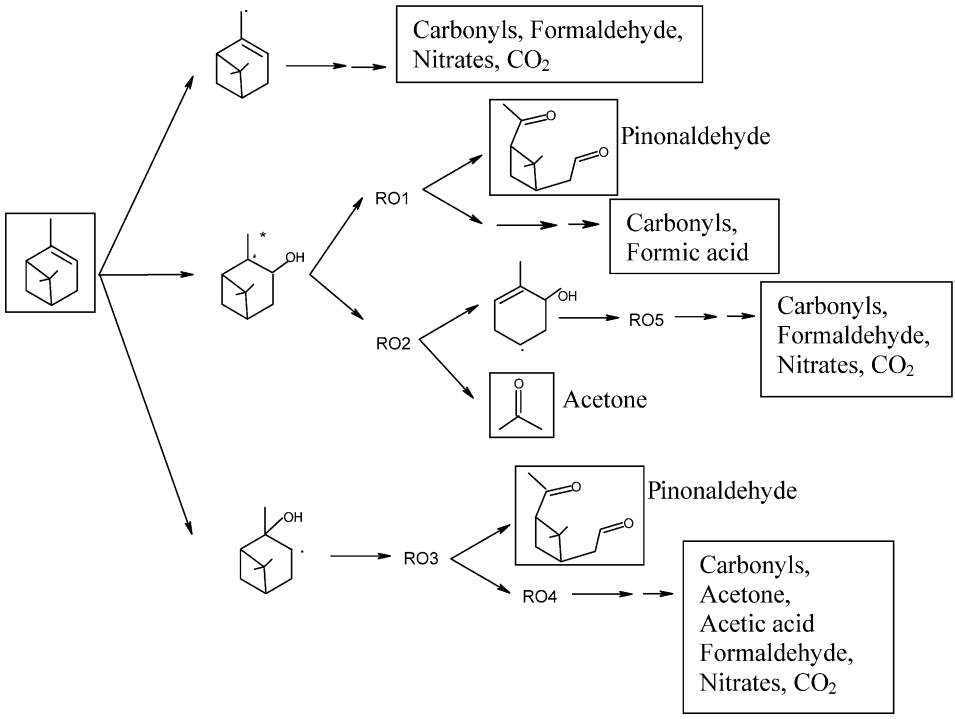

FIGURE 10.12 Mechanistic diagram of the reactions between OH and α-pinene (RO1–RO5 represent the various alkoxy radicals formed in the reactions).

Fan *et al.* [147] found that the OH addition to both pinenes proceeds without an activation barrier, in contrast to a well-defined transition state (for β-pinene only) with level-of-theory dependent barriers reported by Ramirez-Ramirez *et al.* [148]. Fan *et al.* [147] pointed out that the bond lengths (2.7–2.8 Å) of the reaction coordinate in the loose transition states determined by the CVTST is much longer than those (2.1–2.2 Å) in the tight transition states reported by Ramirez-Ramirez *et al.* for β-pinene [148]. The transition states reported by Ramirez-Ramirez *et al.* suffer from high spin contamination so that the geometries of the transition states and the activation energies of the reactions are less reliable. Fan *et al.* reported a rate constant of 5.0×10^{-11}, 6.1×10^{-11} cm^3 $molecule^{-1}$ s^{-1} at B3LYP/6-31G(d,p) level for α- and β-pinene respectively, consistent with the recommended experimental rate constants [149–152]. Peeters *et al.* [153] presented a detailed mechanism for the OH-initiated oxidation of α-pinene in the presence of NO_x using various theoretical methods, e.g., structure–activity relationship (SAR) (It is wide used to model the correlation between the chemical activity and the structure of a family compounds. Such models can be used to predict the activity of an unknown compound based on its structure), quantum chemical methods, transition state theory (TST), and RRKM/master equation analysis. OH addition to the C=C bond accounts for 88% of the reaction, leading to two chemically activated β-hydroxylalkyl rad-

icals with nearly equal branching ratios. H-abstraction channel is found to be a minor route (~12%), but contributes significantly to the overall yield of formaldehyde. The overall product distribution under the simulation conditions are predicted on a molar basis: 35.7% pinonaldehyde, 18.8% formaldehyde, 19% organic nitrates, 17.9% acetone, 25.9% other (hydroxy)carbonyls, 17.2% C1 and C2 carboxylic acids, and 30.7% CO_2, in general agreement with experimentally measured yields. However, under low NO_x conditions the theoretically predicted yields differ significantly, with 59.5% pinonaldehyde, 12.6% formaldehyde, 13.1% organic nitrates, 11.9% acetone, 16.4% other (hydroxy) carbonyls, 8.7% CO_2, and a negligible fraction of C1 and C2 carboxylic acids, possible due to the dominance self- and cross-reactions of the peroxy radicals under low NO_x conditions, which current mechanisms are not able to accurately represent. This theoretical study outlined a comprehensive mechanism and provided a detailed product distribution for the OH-initiated oxidation of α-pinene.

The gas-phase products and mechanisms of OH-initiated oxidation of the pinenes have been explored by numerous experimental studies. Pinonaldehyde from α-pinene and nopinone from β-pinene are observed and quantified as the most abundant products in the gas phase, with a yield of 6% to 87% for pinonaldehyde [154–162] and 17% to 25% for nopinone [160,161,163], respectively. Significant discrepancy exists regarding the reported pinonaldehyde yield from α-pinene, with different analytic techniques and photochemical conditions. The mechanisms leading to the formation of pinonaldehyde and nopinone have been proposed. The resultant β-hydroxylalkyl radicals from addition of OH radicals to the C=C double bond of α-pinene results react rapidly with O_2 and subsequent reactions with NO form β-hydroxylaloxy radicals. The C–C bond fragmentation and subsequent abstraction by O_2 produce pinonaldehyde. For nopinone from β-pinene, a primary and a tertiary β-hydroxylaloxy radical are formed in a similar way as α-pinene, followed by C–C bond scission and subsequent abstraction by O_2, leading to the formation of nopinone, with formaldehyde as co-product. Several studies have reported theoretically predicted yields of pinonaldehyde, with a value of 67% by Fan *et al.* [147], 60% by Peeters *et al.* [153]. A nopinone yield of 23% is predicted by Fan et al [147]. The subsequent oxidations of pinonaldehyde and nopinone by OH radicals have been investigated theoretically. Fantechi *et al.* [163] developed a detailed mechanism of product formation in atmospheric conditions for six H-abstraction sites of pinonaldehyde–OH reaction using SARs, quantum chemistry methods, and TST or RRKM/ME analysis. They found that the overall predicted product yields under high-NO conditions are 22.9% (4-hydroxynorpinonaldehyde), 9.9% (acetone), 12.9% (formaldehyde), 30.3% (organic nitrates), 73.8% (CO_2), 11.4% (HC(O)OH), 16.6% (norpinonaldehyde and CO), and 16.6% (other (hydroxy)(poly)carbonyls). Under lower NO conditions, the theoretically predicted yields differ only regarding 4-hydroxynorpinonaldehyde (38.2%), HC(O)OH (0.3%), and nitrates (26.2%). Lewis *et al.* [164] presented a theoretical study of OH–nopinone reaction and obtained branching ratios of H-abstraction from seven different positions. They found that the most preferable abstraction is at the bridgehead position, with a branching ratio of 23%, inconsistent with the one derived from SARs, which suggests much less oxidation in this position. However,

the results are in agreement with available experimental evidence [165], suggesting formation of significant amounts of products such as 1-hydroxynopinone during terpene oxidation. Calculated rate coefficients using density functional theory with the KMLYP functional are surprisingly in good agreement with the experimental results, possibly because the KMLYP method is a hybrid DFT method with a combination of exchange and correlation functional to minimize the errors for the hydrogen atoms, while preserving the correct asymptotic values.

Another important product from both pinenes oxidation is acetone, an important source of HO_x in the upper troposphere [166] and low stratosphere and also an important precursor for peroxyacetyl-nitrate (PAN) in the atmosphere [167]. Acetone formation from both pinenes has been experimentally determined, with a yield of 5–18% from α-pinene [157–159,168–170] and 2–13% from β-pinene [159, 160,168–170]. Several mechanisms have been proposed for the formation of acetone from OH-initiated oxidation of α- and β-pinene. A theoretical study by Vereecken and Peeters [171] showed that the initial OH-addition reaction leads to the formation of chemically activated tertiary β-hydroxylalkyl radicals with an initial internal energy of 32 kcal mol^{-1}. Subsequent prompt isomerization of the activated radicals to 6-hydroxymenthen-8-yl is comparable to the thermal stabilization according to the kinetic calculations using RRKM/ME. The resultant radical (6-hydroxymenthen-8-oxy) reacts with O_2 and NO and subsequent decomposition of the β C=C bond provide one possible route for formation of acetone. Figure 10.13 shows the major formation mechanism of acetone from OH–α-pinene reactions. The authors reported an acetone yield of 8.5%, in agreement with available experimental data [157–159,168–170]. This channel is also confirmed by Dibble [172] in a theoretical study: the activation energy of ~8-12 kcal mol^{-1} is obtained for the rearrangement of the tertiary β-hydroxylalkyl radical, which is crucial for subsequent formation of acetone. An alternative pathway for acetone formation has been proposed, involving C–C (either one of C–C bonds connected to the radical center) scission of the tertiary β-hydroxylalkoxy radical, followed by alkoxy radical formation via reaction with O_2 and NO and subsequent decomposition, leading to the formation of acetone. A less possible pathway for the formation of acetone is suggested via OH abstraction, which has been demonstrated to be implausible in a theoretical study by Vereecken and Peeters [171]

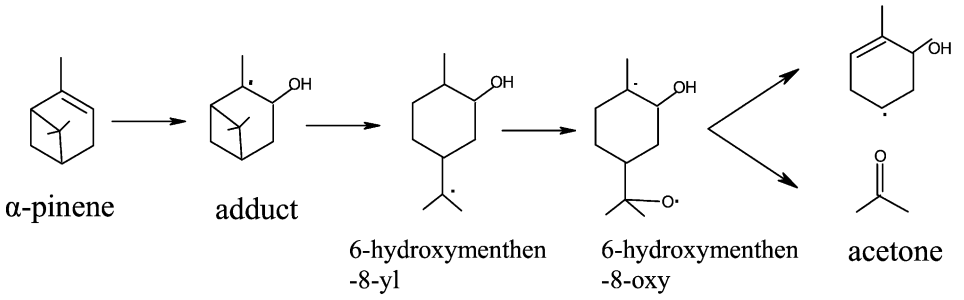

FIGURE 10.13 Major channel of acetone formation from OH–α-pinene reactions.

due to the constraints of the bicyclo skeleton. Fan *et al.* [147] predicted a yield of 9.5% for acetone from OH–α-pinene reaction. Similar mechanisms for the formation of acetone from β-pinene have been proposed via OH-addition channel (tertiary OH–β-pinene adduct). Several other gas-phase products (e.g., formaldehyde, nitrates, hydroxycarbonyls) are also observed and quantified with various yields. For example, formaldehyde is quantified with a molar yield of 19% and 23% [158,170] for α-pinene and 45% and 54% for β-pinene [155,170]. Organic nitrates have been quantified only in two experiments, with the yield of 1% [154] and 18% [157], showing significant disagreement. The mechanisms leading to these products have been proposed, although remain to be scrutinized. A detailed gas-phase mechanism [173] for the degradation of α-pinene by OH has been proposed based on box model simulations of laboratory measurements performed in the presence as well as in the absence of NO by Noziere *et al.* [158]. The results showed that the levels of OH, NO, NO_2 are well reproduced in the model and the model succeeds in reproducing the average apparent yields of pinonaldehyde, acetone, total nitrates and total PANs in the experiments performed in the presence of NO. In the absence of NO, pinonaldehyde is fairly well reproduced, but acetone is largely underestimated. The results also showed that the main oxidation channels differ largely according to photochemical conditions. The pinonaldehyde yield is estimated to be about 10% in the remote atmosphere and up to 60% in very polluted areas. This finding explained the large existing discrepancy for the measured pinonaldehyde yield reported previously [154–161].

As previously mentioned in the OH–isoprene reaction, the ring-closure reaction in both unsaturated peroxy- and oxy radicals are expected to be important pathways in the atmospheric chemistry of the OH–pinenes system. Vereecken and Peeters [89] predicted a peroxy ring-closure rate constant of 2.6 s^{-1} at 298 K, well above the rate of the NO reaction even at 1 ppbv NO and those with HO_2/RO_2 at the atmospheric concentrations. The formation of ring closure peroxide not only changes the product distribution, e.g., reducing acetone formation, but also these peroxides are highly oxygenated and hence low volatile, contributing to SOA formation. For the unsaturated structures discussed above, the resulting oxy radical RO likely undergoes ring closure, forming cyclic ether structures. For example, the oxy radicals form from α-pinene after opening of the 4-membered ring and subsequent reactions with O_2 and NO. The oxy radical site can attack the double bond, forming a cyclic ether radical which can in turn react quickly with O_2 to form a cycloetherperoxy radical. However, this new channel is not currently well-understood and more systematic investigation is needed in order to better understand this unique channel.

Ozonolysis of pinenes contributes to OH radical and SOA formation. The latter has been speculated to be responsible for the formation of "blue haze". Hence, it is of vital importance to quantitatively understand the roles of ozonolysis of α- and β-pinenes on both OH and SOA formation in the troposphere. The O_3 reaction with both pinenes follows the Criegee mechanism, similar to that of isoprene. The initial step proceeds through cycloaddition of O_3 to the C=C double bond of each pinene, forming a primary ozonide (POZ). The available reaction energy is retained as the internal energy of the product, resulting in formation

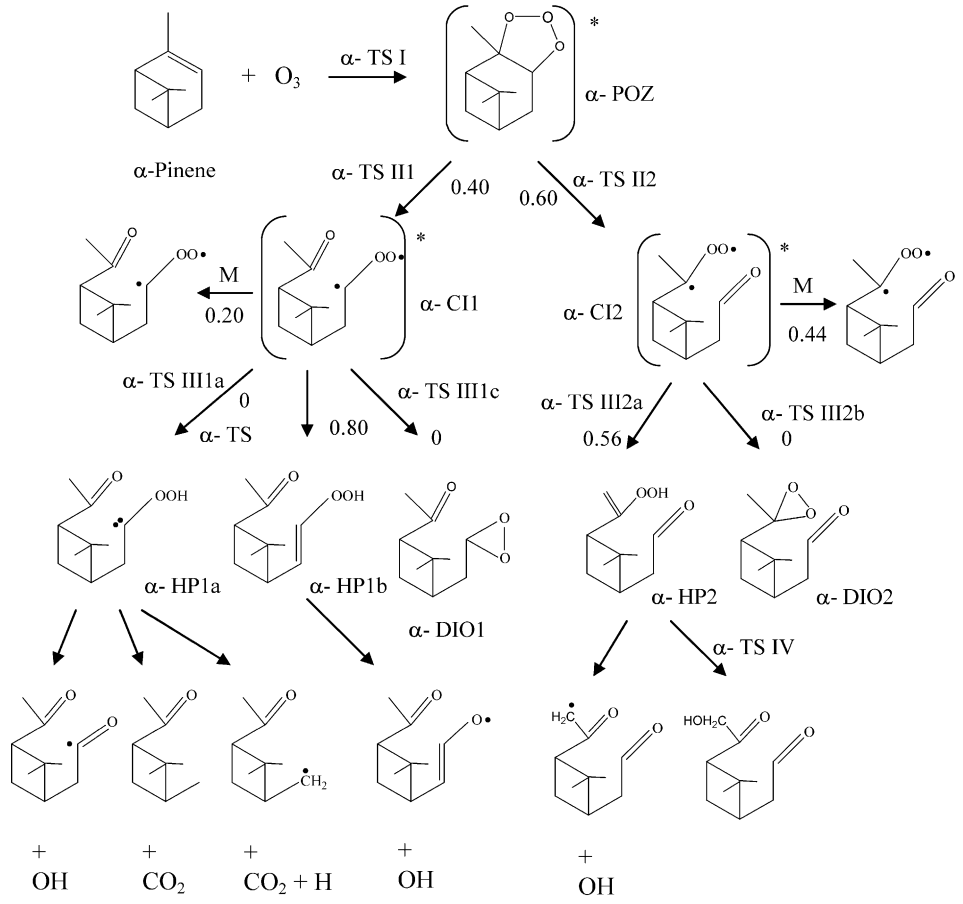

FIGURE 10.14 Mechanistic diagram of ozonolysis of α-pinene.

of the vibrationally excited primary ozonide. The excited primary ozonide subsequently undergoes unimolecular isomerization (for α-pinene) or decomposition (for β-pinene) to yield chemically activated carbonyl oxides and/or aldehydes (for β-pinene). A large fraction of the carbonyl oxides have ample internal energy and are subjected to prompt unimolecular reactions or collisional stabilization. Two reaction pathways were proposed for the carbonyl oxide, ring closure to form dioxirane or H-migration to produce a hydroperoxide intermediate. The hydroperoxide subsequently undergoes isomerization or decomposition, leading to formation of OH, carbonyls, CO_2, and a variety of other products, some of which are potential SOA precursors. Thermally stabilized CIs may react with other atmospheric compounds (e.g., H_2O, SO_2, HCHO, H_2SO_4). Numerous experiments have been carried out to investigate the products and SOA formation from ozonolysis of pinenes [174–179]. However, only one theoretical study has been reported for ozonolysis of pinenes. Zhang and Zhang [180] presented a comprehensive theoretical study of the reactions of ozone with α- and β-pinenes using combined quantum-chemical

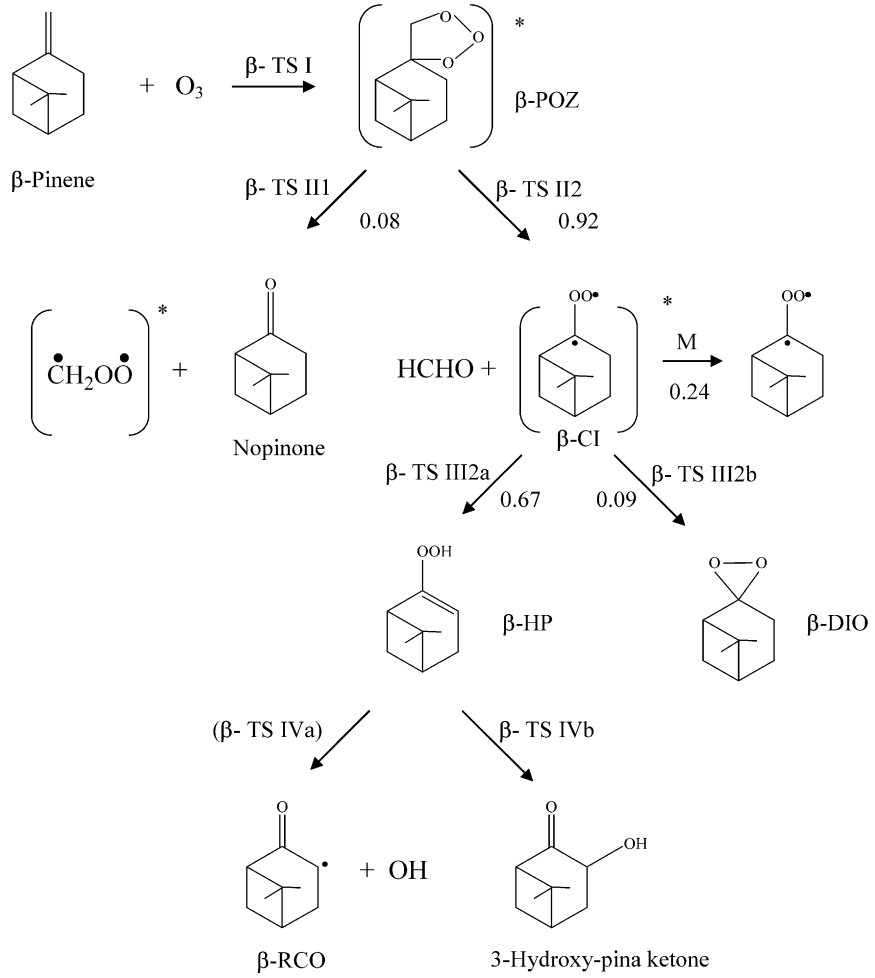

FIGURE 10.15 Mechanistic diagram of ozonolysis of β-pinene.

methods (e.g., DFT and CCSD(T)) and RRKM/ME to determine the structures and energetics of relevant species in the reaction systems and to predict the kinetics and mechanisms of pinenes ozonolysis. Figures 10.14 and 10.15 represent the mechanistic diagrams of the ozonolysis of α-, β-pinene, respectively. The formation of POZs occurs with the activation barriers of 0.3 kcal mol^{-1} for α-POZ and 2.0 kcal mol^{-1} for β-POZ. The addition reactions are highly exothermic, with the reaction energies of 55.1 and 51.1 kcal mol^{-1} for α- and β-pinenes, respectively. The results indicate a negligible collision stabilization of the POZs. Cleavage of both POZs forms two carbonyl oxides along with aldehyde or ketone, respectively. For both activated and stabilized CIs from α- and β-pinene ozonolysis, H-migration to hydroperoxides dominates over ring closure into dioxirane. Significant fractions of CIs are stabilized with 0.34 for α-CIs and 0.22 for β-CI, consistent with

the experimental observations. The theoretical calculations suggest that stabilized CIs contribute significantly to previously measured high yield of OH for α-pinene, but stabilized CIs contribute negligibly to the experimental OH yield for β-pinene because of the reaction with formaldehyde.

Reaction with NO_3 radicals represents another important gas phase loss pathway for α-pinene during the night time. Under elevated NO_x conditions, reaction with NO_3 can also be significant during the daytime and contribute substantially to the monoterpene decay. However, only a few studies have been performed on NO_3-initiated oxidation of pinenes [181–184]. To our knowledge, no theoretical studies have been performed to investigate the mechanistic behaviors of these reactions.

3.3 Other monoterpenes and sesquiterpenes

The α- and β-pinenes with other monoterpenes ($C_{10}H_{16}$) naturally-emitted into the troposphere from vegetation is comparable to or can even exceed the emissions of nonmethane organic compounds from anthropogenic sources on a regional and global scale. There are evidences that show significant amounts of OH radicals formed from reaction of monoterpenes with ozone. The monoterpene is very reactive toward OH radical with a typical lifetime of about several hours in the atmosphere. The intermediates and products produced from monoterpene oxidation also contribute to the ozone and secondary aerosol formation in the troposphere. Theoretical studies on other monoterpenes than pinenes are sparse in the literature and only a few are discussed in this review. Carrasco *et al.* [185] performed both experimental and theoretical study to investigate gas phase OH-initiated sabinene reaction. Three primary carbonyl products (acetone, sabinaketone and formaldehyde) have been observed and quantified in the absence and presence of NO_x. Quantum chemical DFT-B3LYP calculations reveal that both abstraction and addition channel need to be taken into account for acetone production and sabinaketone and formaldehyde are the mainly products of the addition channels. The results also indicate that DFT is an appropriate level of theory with reasonable reliability and computational cost for such a large reaction system. Their previous studies showed that barrier heights calculated at the DFT-B3LYP are good agreement with experimental results and the high level *ab initio* calculations. Semi-empirical parameters obtained from correlation between Cl and simple monoalkene and dienes were used to predict the rate constants of Cl atom and a series of monoterpenes including α-pinene, 2-carene, 3-carene, myrcene, and γ-terpinene, based on the framework of perturbation molecular orbital (PFMO) theory [186]. The HOMO energies were calculated using *ab initio* and DFT quantum chemical methods. The calculated rate constants were found to be generally in agreement with available literature values. Ramirez-Ramirez and Nebot-Gil [187] carried out *ab initio* calculations to investigate the initial step of the gas-phase OH–*d*-limonene reaction by considering eight different possibilities for OH addition to the endo and exo C=C double bonds with syn or anti configuration (Figure 10.16). Activation energies calculated at the QCISD(T)/6-31G(d)//UMP2/6-31G(d) level show that OH is preferably added to endocyclic C=C bond under atmospheric

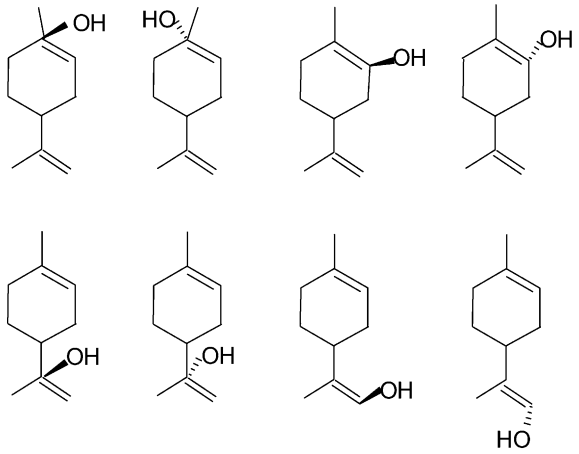

FIGURE 10.16 Schematic diagram of the eight OH–*d*-limonene adduct isomers.

conditions. The gas-phase basicity (GB) and proton affinity (PA) of limonene were calculated based on the density functional methods with best predicted values of 869.6 and 873.9 kJ mol^{-1} for PA at B3PW91/6-31G* and BLYP/6-31G* respectively, in agreement with the measure value (875.5 kJ mol^{-1}) [188], providing valuable information for the measurement of this compound in the atmosphere.

In recent years, increasing interests have arisen for sesquiterpenes ($C_{15}H_{24}$) due to the fact that oxidation of these terpenes has potentially significant contribution to biogenic SOA formation. However, theoretical studies of sesquiterpenes are very limited and only one study concerning the molecular conformations of β-caryophyllene has been reported [189]. Four conformations of β-caryophyllene ($\alpha\alpha$, $\alpha\beta$, $\beta\alpha$, and $\beta\beta$) were investigated by means of *ab initio* calculations at several levels of theory (e.g., HF/6-31G*, MP2/6-31G*, and B3LYP/6-31G*) to investigate their relative thermodynamic stabilities. The results predicted that the $\alpha\alpha$ conformer corresponds to the most stable geometry, in agreement with low-temperature NMR measurements.

4. CONCLUSIONS AND FUTURE RESEARCH

During the past two decades there has been significant progress in the application of quantum chemical calculations to the field of atmospheric chemistry. In this article, we have presented an overview of the application of quantum chemical calculations and kinetic methods to elucidate the mechanism of atmospheric biogenic hydrocarbon oxidations. Recent advances in isoprene and α-, β-pinenes are discussed in this review. The mechanism of isoprene oxidation is better understood than those of other biogenic hydrocarbons. The initial isoprene-oxidant adducts, the peroxy radicals, the alkoxy radicals and the first generation products are investigated by means of quantum chemical calculations. The roles of the intermediate species are assessed using kinetic methods and the overall picture of the isoprene

oxidation mechanism is obtained. For pinenes, monoterpenes, and sesquiterpenes, there have been limited theoretical studies on the kinetics and mechanism of these systems initiated by oxidants such as OH and O_3. Consequently, large uncertainty exists on the atmospheric oxidation of these biogenic VOCs.

Typically, several aspects need to be considered for application of quantum chemical calculations and kinetic methods to the atmospheric biogenic hydrocarbons:

(1) The accuracy of the geometries of the species. A reliable potential energy surface depends on reliable geometries of reactants, transition states, intermediates, and products. For biogenic hydrocarbons (e.g., isoprene, α-, β-pinenes), it is difficult or formidable to determine their geometries experimentally. In most of the hydrocarbon oxidation systems, density functional methods have been proven to be an efficient approach, which accurately predicts structural parameters (e.g., bond length, bond angle, and dihedral angle) considering the relatively low computational cost of the methods and have been validated in many applications. Higher level theories have been employed to obtain more accurate structural requirement by balancing between accuracy and computational efficiency. The MP2 and G2 levels are also frequently employed in geometry optimization of species from atmospheric hydrocarbons oxidation.
(2) The accuracy of the reaction energy and activation energy. Quantum chemical calculations provide a simple way to compute the reaction energy/enthalpy and activation energy for a reaction in the biogenic hydrocarbon oxidation system. The theoretical results are needed to be compared with available experimental values. In most cases, higher levels of calculations than DFT calculations (e.g., Gaussian series of theory) are required to obtain accurate energy profiles, especially for the activation energy, which is needed in predicting the reaction rate constant. Once the reaction energy and the activation energy are accurately defined, a reliable potential energy surface is established. For reactions proceeding without barriers, accurate reaction energy, geometry, vibrational frequencies are required to model the potential energy surface using variational transition state theory.
(3) Other thermochemical data (e.g., heat of formation and proton affinity). These thermochemical data are very helpful to atmospheric modeling to understand the complex chemical reactions. Thermochemical data can be obtained by high levels of calculations, e.g., CCSD(T), Gn series, CBS, QCI, etc.
(4) Kinetic theories. The high-pressure limit rate constants can be determined using classic kinetic theory, e.g., TST for tight transition states and CVTST for loose transition states. Kinetic methods such as RRKM or vRRKM can be employed to investigate the temperature and pressure dependent behaviors in fall-off region. RRKM (or vRRKM) in conjunction with master equation is used to evaluate the competition between prompt chemical reactions and collisional stabilization of the excited species. Separate statistical ensemble (SSE) approach can be used to determine the energy partitioning from the parent species into its fragments. The accuracies of the rate constants determined from various kinetic rate methods strongly depend on the accuracies of the

predicted barrier height and vibration frequencies of the transition states and the reactants.

(5) The fates of chemically activated intermediate species. For many oxidation reactions encountered in biogenic hydrocarbon oxidation, especially ozonolysis of isoprene and monoterpene, large excessive energy is released, resulting in the formation of highly excited intermediate species. The fates of these species can be evaluated by RRKM or vRRKM/ME formulism and the energy can be further partitioned into the decomposition products according to the SSE theory.

As the late Nobel laureate John A. Pople [190] pointed out almost ten years ago that "the reaction mechanisms with pollutants in the atmosphere could be studied using computational chemistry". Today, more studies have been undertaken by exploiting quantum chemical calculations and chemical kinetic methods to investigate the oxidation mechanisms of volatile organic compounds in the atmosphere. Quantum chemical calculations and theoretical kinetic models serve as the guidance and support for experimental research. The theoretical framework has been developed over many decades and the maturation of concepts, methods, and algorithms have been validated in the field of atmospheric chemistry. High-level calculations for large organic molecular systems are still computationally demanding and extremely challenging for atmospheric theoretical investigators. However, with the development of high-performance computational facility and better mathematical algorithms, such difficulties and challenges will be overcome in the near future.

ACKNOWLEDGEMENTS

This work was supported by the Robert A. Welch Foundation (Grant A-1417). Additional support was provided by the Texas A&M University Supercomputing Facilities. The authors also acknowledge the use of the Laboratory for Molecular Simulations at Texas A&M University.

REFERENCES

[1] A. Guenther, C.N. Hewitt, D. Erickson, R. Fall, C. Geron, T. Graedel, P. Harley, L. Klinger, M. Lerdau, W.A. McKay, T. Pierce, B. Scholes, R. Steinbrecher, R. Tallamraju, J. Taylor, P.J. Zimmermann, *J. Geophys. Res.* **100** (1995) 8873.

[2] A. Guenther, C. Geron, T. Pierce, B. Lamb, P. Harley, R. Fall, *Atmos. Environ.* **34** (2000) 2205.

[3] R. Fall, in: C.N. Hewitt (Ed.), *Reactive Hydrocarbons in the Atmosphere*, Academic Press, San Diego, 1999, pp. 41–96.

[4] J.D. Fuentes, M. Lerdau, R. Atkinson, D. Baldocchi, J.W. Bottenheim, P. Ciccioli, B. Lamb, C. Geron, L. Gu, A. Guenther, T.D. Sharkey, W. Stockwell, *Bull. Am. Meteorol. Soc.* **81** (2000) 1537.

[5] J. Finlayson-Pitts, J.N. Pitts Jr., *Chemistry of the Upper and Lower Atmosphere: Theory, Experiments, and Applications*, Academic Press, San Diego, CA, 2000.

[6] J.H. Seinfeld, S.N. Pandis, *Atmospheric Chemistry and Physics: From Air Pollution to Climate Change*, Wiley, New York, 1997.

[7] R. Zhang, W. Lei, X. Tie, P. Hess, *Proc. Natl. Acad. Sci. USA* **101** (2004) 6346.

[8] R. Zhang, I. Suh, J. Zhao, D. Zhang, E.C. Fortner, X. Tie, L.T. Molina, M.J. Molina, *Science* **304** (2004) 1487.
[9] W. Lei, R. Zhang, X. Tie, P. Hess, *J. Geophys. Res.* **109** (2004) D12301, doi:10.1029/2003JD004219.
[10] J. Fan, R. Zhang, G. Li, J. Nielsen-Gammon, Z. Li, *J. Geophys. Res.* **110** (2005) D16203, doi:10.1029/2005JD005805.
[11] R. Atkinson, J. Arey, *Atmos. Environ.* **37** (2003) S197.
[12] R. Atkinson, *Atmos. Environ.* **24** (1990) 1.
[13] R. Atkinson, *J. Phys. Chem. Ref. Data* **26** (1997) 215.
[14] R. Atkinson, D.L. Baulch, R.A. Cox, J.N. Crowley, R.F. Hampson, R.G. Hynes, M.E. Jenkin, M.J. Rossi, J. Troe, *Atmos. Chem. Phys.* **6** (2006) 3625.
[15] G. Li, R. Zhang, J. Fan, X. Tie, *J. Geophys. Res.* **112** (2007) D10309, doi:10.1029/2006JD007924.
[16] F. Jensen, *Introduction to Computational Chemistry*, 2nd ed., Wiley, Hoboken, NJ, 2007.
[17] W. Koch, M.C. Holthausen, *A Chemist's Guide to Density Functional Theory*, Willey–VCH, New York, 2000.
[18] M.A.L. Marques, E.K.U. Gross, *Annu. Rev. Phys. Chem.* **55** (2004) 427.
[19] R.O. Jones, O. Gunnarsson, *Rev. Mod. Phys.* **61** (1989) 681.
[20] S. Kristyan, P. Pulay, *Chem. Phys. Lett.* **229** (1994) 175.
[21] Y. Anderson, D.C. Langreth, C.A. Gonzales, P.M.W. Gill, J.A. Pople, *Chem. Phys. Lett.* **221** (1994) 100.
[22] J. Cizek, *J. Chem. Phys.* **45** (1966) 4256.
[23] R. Krishnan, J.A. Pople, *Int. J. Quantum Chem.* **14** (1978) 91.
[24] R. Krishnan, M.J. Frisch, J.A. Pople, *J. Chem. Phys.* **72** (1980) 4244.
[25] J.A. Pople, M. Headgordon, K. Raghavachari, *J. Chem. Phys.* **87** (1987) 5968.
[26] K. Raghavachari, J.A. Pople, E.S. Replogle, M. Headgordon, *J. Phys. Chem.* **94** (1990) 5579.
[27] J.R. Bartlett, Couple Cluster theory: An overview of recent developments, in: D.R. Yarkony (Ed.), *Modern Electronic Structure Theory*, Part II, World Scientific, Singapore, 1995.
[28] J.W. Ochterski, G.A. Petersson, J.A. Montgomery, *J. Chem. Phys.* **104** (1996) 2598, and references therein.
[29] L.A. Curtiss, P.C. Redfern, K. Raghavachari, *J. Chem. Phys.* **126** (2007), Art. No. 084108, and references therein.
[30] T. P Lee, P.R. Taylor, *Int. J. Quantum Chem. Suppl.* **23** (1989) 199.
[31] J.C. Rienstra-Kiracofe, W.D. Allen, H.F. Schaefer III, *J. Phys. Chem. A* **104** (2000) 9823.
[32] M. Hotokka, B. Roos, P. Siegbahn, *J. Am. Chem. Soc.* **105** (1983) 5263.
[33] O. Roos, The complete active space self-consistent field method and its applications in electronic structure calculations, in: K.P. Lawley (Ed.), *Ab Initio Methods in Quantum Chemistry*, Part II, Wiley, New York, 1987, pp. 399–445.
[34] R. Shapard, The mutliconfiguration self-consistent field method, in: K.P. Lawley (Ed.), *Ab Initio Methods in Quantum Chemistry*, Part II, Wiley, New York, 1987, pp. 63–200.
[35] Y.Y. Chuang, E.L. Coitino, D.G. Truhlar, *J. Phys. Chem. A* **104** (2000) 446.
[36] R.G. Parr, W. Yang, *Density Functional Theory of Atoms and Molecules*, Oxford University Press, New York, 1989.
[37] H. Nakano, K. Hir, *Bull. Korean Chem. Soc.* **24** (2003) 812.
[38] M. Alcami, O. Mo, M. Yanez, *Mass Spectrom. Rev.* **20** (2001) 195.
[39] O. Christiansen, *Theor. Chem. Acc.* **116** (2006) 106.
[40] M. Garavelli, *Theor. Chem. Acc.* **116** (2006) 87.
[41] K.J. Laidler, M.C. King, *J. Phys. Chem.* **87** (1983) 2657.
[42] G. Truhlar, W.L. Hase, J.T. Hynes, *J. Phys. Chem.* **87** (1983) 2664.
[43] G. Truhlar, B.C. Garrett, S.J. Klippenstein, *J. Phys. Chem.* **100** (1996) 12771.
[44] J.I. Steinfeld, J.S. Francisco, W.L. Hase, *Chemical Kinetics and Dynamics*, Prentice Hall, Upper Saddle River, NJ, 1999.
[45] D.G. Truhlar, B.C. Garrett, *Acc. Chem. Res.* **13** (1980) 440.
[46] D.G. Truhlar, B.C. Garrett, *Annu. Rev. Phys. Chem.* **35** (1984) 159.
[47] W.L. Hase, *Chem. Phys. Lett.* **139** (1987) 389.
[48] K. Holbrook, M. Pilling, S. Robertson, *Unimolecular Reactions*, Wiley, Chichester, UK, 1996.
[49] R.G. Gilbert, S.C. Smith, *Theory of Unimolecular and Recombination Reactions*, Blackwell Scientific, Oxford, UK, 1990.

[50] T. Baer, W.L. Hase, *Unimolecular Reaction Dynamics: Theory and Experiments*, Oxford University Press, New York, 1996.
[51] D. Zhang, R. Zhang, J. Park, S.W. North, *J. Am. Chem. Soc.* **124** (2002) 9600.
[52] J.Y. Zhang, T. Dransfield, N.M. Donahue, *J. Phys. Chem. A* **108** (2004) 9082.
[53] M. Olzmann, E. Kraka, D. Cremer, R. Gutbrod, S. Andersson, *J. Phys. Chem. A.* **101** (1997) 9421.
[54] J.H. Kroll, S.R. Sahay, J.G. Anderson, K.L. Demerjian, N.M. Donahue, *J. Phys. Chem. A* **105** (2001) 4446.
[55] C. Wittig, I. Nadler, H. Reisler, M. Nobel, J. Catanzarite, G. Radhakrishnan, *J. Chem. Phys.* **83** (1985) 5581.
[56] J.J. Orlando, G.S. Tyndall, L. Vereecken, J. Peeters, *J. Phys. Chem. A* **104** (2000) 11578.
[57] L. Bunker, W.L. Hase, *J. Chem. Phys.* **59** (1973) 4621.
[58] G. Vayner, S.V. Addepalli, K. Song, W.L. Hase, *J. Chem. Phys.* **125** (2006) 014317.
[59] M. Trainer, E.J. Williams, D.D. Parrish, M.P. Buhr, E.J. Allwine, H.H. Westberg, F.C. Fehsenfeld, S.C. Liu, *Nature* **329** (1987) 705.
[60] R.A. Rasmussen, M.A. Khalil, *J. Geophys. Res.* **93** (1988) 1417.
[61] S. Madronich, J.G. Calvert, *J. Geophys. Res.* **95** (1990) 5697.
[62] R.D. Lightfoot, R.A. Cox, J.N. Crowley, M. Destriau, G.D. Hayman, M.E. Jenkin, G.K. Moortgat, F. Zabel, *Atmos. Environ.* **26** (1992) 1805.
[63] M.E. Jenkin, S.M. Saunders, M.J. Pilling, *Atmos. Environ.* **31** (1997) 81.
[64] M.E. Jenkin, A.A. Boyd, R. Lesclaux, *J. Atmos. Chem.* **29** (1998) 267.
[65] T.S. Dibble, *J. Phys. Chem. A* **103** (1999) 8559.
[66] W.F. Lei, R.Y. Zhang, *J. Phys. Chem. A* **105** (2000) 3808.
[67] T.S. Dibble, *J. Phys. Chem. A* **108** (2004) 2208.
[68] J. Zhao, R.Y. Zhang, E.C. Fortner, S.W. North, *J. Am. Chem. Soc.* **126** (2004) 2686.
[69] J. Fan, R. Zhang, *Environ. Chem.* **1** (2004) 140.
[70] S. McGivern, I. Suh, A.D. Clinkenbeard, R. Zhang, S.W. North, *J. Phys. Chem. A* **104** (2000) 6609.
[71] W. Lei, R. Zhang, W.S. McGivern, A. Derecskei-Kovacs, S.W. North, *Chem. Phys. Lett.* **326** (2000) 109.
[72] W. Lei, A. Derecskei-Kovacs, R. Zhang, *J. Chem. Phys.* **113** (2000) 5354.
[73] R. Zhang, W. Lei, *J. Chem. Phys.* **113** (2000) 8574.
[74] P. Campuzano-Jost, M.B. Williams, L. D'Ottone, A.J. Hynes, *Geophys. Res. Lett.* **27** (2000) 693.
[75] P.S. Stevens, E. Seymour, Z.J. Li, *J. Phys. Chem. A* **104** (2000) 5989.
[76] R. Zhang, I. Suh, W. Lei, A.D. Clinkenbeard, S.W. North, *J. Geophys. Res.* **105** (2000) 24627.
[77] B. Chuong, P.S. Stevens, *J. Phys. Chem. A* **104** (2000) 5230.
[78] J. Park, C.G. Jongsma, R. Zhang, S.W. North, *Phys. Chem. Chem. Phys.* **5** (2003) 3638.
[79] M. Francisco-Marquez, J.R. Alvarez-Idaboy, A. Galano, A. Vivier-Bunge, *Phys. Chem. Chem. Phys.* **5** (2003) 1392.
[80] M. Francisco-Marquez, J.R. Alvarez-Idaboy, A. Galano, A. Vivier-Bunge, *Environ. Sci. Technol.* **39** (2005) 8797.
[81] W. Lei, R. Zhang, W.S. McGivern, A. Derecskei-Kovacs, S.W. North, *J. Phys. Chem. A* **105** (2001) 471.
[82] M.E. Jenkin, G.D. Hayman, *J. Chem. Soc. Faraday Trans.* **91** (1995) 1911.
[83] S.E. Paulson, J.H. Seinfeld, *J. Geophys. Res.* **97** (1992) 20703.
[84] D. Zhang, R. Zhang, C. Church, S.W. North, *Chem. Phys. Lett.* **343** (2001) 49.
[85] J. Park, C.G. Jongsma, R. Zhang, S.W. North, *J. Phys. Chem. A* **108** (2004) 10688.
[86] V.M. Ramirez-Ramirez, I. Nebot-Gil, *Int. J. Quantum Chem.* **105** (2005) 518.
[87] J. Park, J.C. Stephens, R. Zhang, S.W. North, *J. Phys. Chem.* **107** (2003) 6408.
[88] J.E. Reitz, W.S. McGivern, M.C. Church, M.D. Wilson, S.W. North, *Int. J. Chem. Kinet.* **34** (2002) 255.
[89] L. Vereecken, J. Peeters, *J. Phys. Chem. A* **108** (2004) 5197.
[90] K.N. Houk, K.R. Condroski, W.A. Pryor, *J. Am. Chem. Soc.* **118** (1996) 13002.
[91] R. Cameron, A.M.P. Borrejo, B.M. Bennett, G.R.J. Thatcher, *Can. J. Chem.* **73** (1995) 1627.
[92] B.S. Jursic, L. Klasine, S. Pecur, W.A. Pryor, *Nitric Oxide* **1** (1997) 494.
[93] J.M. O'Brien, E. Czuba, D.R. Hastie, J.S. Francisco, P.B. Shepson, *J. Phys. Chem. A* **102** (1998) 8903.
[94] J. Zhao, R. Zhang, S.W. North, *Chem. Phys. Lett.* **369** (2003) 204.

[95] J. Yu, H.E. Jeffries, R.M. Le Lacheur, *Environ. Sci. Technol.* **29** (1995) 1923.
[96] S. Kwok, R. Atkinson, J. Arey, *Environ. Sci. Technol.* **29** (1995) 2467.
[97] V.M. Ramirez-Ramirez, I. Nebot-Gil, *Chem. Phys. Lett.* **406** (2005) 404.
[98] T.S. Dibble, *J. Phys. Chem. A* **108** (2004) 2199.
[99] T.A. Biesenthal, J.W. Bottenheim, P.B. Shepson, P.C. Brickell, *J. Geophys. Res.* **103** (1998) 25487.
[100] J.H. Kroll, N.L. Ng, S.M. Murphy, R.C. Flagan, J.H. Seinfeld, *Geophys. Res. Lett.* **32** (2005), Art. No. L18808.
[101] T.E. Kleindienst, M. Lewandowski, J.H. Offenberg, M. Jaoui, E.O. Edney, *Geophys. Res. Lett.* **34** (2007), Art. No. L01805.
[102] R. Atkinson, S.M. Aschmann, J. Arey, B. Shorees, *J. Geophys. Res.* **97** (1992) 6065.
[103] S.M. Aschmann, J. Arey, R. Atkinson, *Atmos. Environ.* **30** (1996) 2939.
[104] R. Gutbrod, S. Meyer, M.M. Rahman, R.N. Schindler, *Int. J. Chem. Kinet.* **29** (1997) 717.
[105] S.E. Paulson, M. Chung, A.D. Sen, G. Orzechowska, *J. Geophys. Res.* **103** (1998) 25333.
[106] P. Neeb, G.K. Moortgat, *J. Phys. Chem. A* **103** (1999) 9003.
[107] R. Gutbrod, E. Kraka, R.N. Schindler, D. Cremer, *J. Am. Chem. Soc.* **119** (1997) 7330.
[108] D. Zhang, R.Y. Zhang, *J. Am. Chem. Soc.* **124** (2002) 2692.
[109] D. Zhang, W.F. Lei, R.Y. Zhang, *Chem. Phys. Lett.* **358** (2002) 171.
[110] K.T. Kuwata, L.C. Valin, A.D. Converse, *J. Phys. Chem. A* **109** (2005) 10710.
[111] S.M. Aschmann, R. Atkinson, *Environ. Sci. Technol.* **28** (1994) 1539.
[112] D. Grosjean, E.L. Williams II, E. Grosjean, *Environ. Sci. Technol.* **27** (1993) 830.
[113] T. Kurten, B. Bonn, H. Vehkamaki, M. Kulmala, *J. Phys. Chem. A* **111** (2007) 3394.
[114] K.H. Becker, K.J. Brockmann, J. Bechara, *Nature* **346** (1990) 256.
[115] K.H. Becker, J. Bechara, K. Brockmann, *J. Atmos. Environ.* **27A** (1993) 57.
[116] R. Simonaitis, K.J. Olsyna, J.F. Meagher, *Geophys. Res. Lett.* **18** (1991) 9.
[117] P. Neeb, F. Sauer, O. Horie, G.K. Moortgat, *Atmos. Environ.* **31** (1997) 417.
[118] F. Sauer, C. Schafer, P. Neeb, O. Horie, G.K. Moortgat, *Atmos. Environ.* **33** (1999) 229.
[119] P. Aplincourt, J.M. Anglada, *J. Phys. Chem. A* **107** (2003) 5798.
[120] P. Aplincourt, J.M. Anglada, *J. Phys. Chem. A* **107** (2003) 5812.
[121] A.B. Ryzhkov, P.A. Ariya, *Phys. Chem. Chem. Phys.* **6** (2004) 5042.
[122] A.B. Ryzhkov, P.A. Ariya, *Chem. Phys. Lett.* **419** (2006) 479.
[123] A. Geyer, B. Alicke, S. Konrad, T. Schmitz, J. Stutz, U. Platt, *J. Geophys. Res.* **106** (2001) 8013.
[124] D.D. Riemer, P.J. Milne, C.T. Farmer, R.G. Zika, *Chemosphere* **28** (1994) 837.
[125] T.K. Starn, P.B. Shepson, S.B. Bertman, D.D. Riemer, R.G. Zika, K. Olszyna, *Geophys. Res. Lett.* **103** (1998) 22437.
[126] I. Suh, W. Lei, R. Zhang, *J. Phys. Chem. A* **105** (2001) 6471.
[127] H. Skov, J. Hjorth, C. Lohse, N.R. Jenen, G. Restelli, *Atmos. Environ.* **26A** (1992) 2771.
[128] T. Berndt, O. Boge, *Int. J. Chem. Kinet.* **29** (1997) 755.
[129] D. Zhang, R. Zhang, *J. Chem. Phys.* **116** (2002) 9721.
[130] J. Zhao, R.Y. Zhang, *Atmos. Environ.*, in press.
[131] J. Zhao, R.Y. Zhang, *J. Phys. Chem. A*, in preparation for publication.
[132] B.T. Jobson, H. Niki, Y. Yokouchi, J. Bottenheim, F. Hopper, R. Leaitch, *J. Geophys. Res.* **99** (1994) 25355.
[133] S. Solberg, N. Schmidbauer, A. Semb, F. Stordal, O. Hov, *J. Atmos. Chem.* **23** (1996) 301.
[134] W. Wingenter, M.K. Kubo, N.J. Blake, T.W. Smith, F.S. Rowland, *J. Geophys. Res.* **101** (1996) 4331.
[135] A.P. Pszeeny, W.C. Keene, D.J. Jacob, S. Fan, J.R. Maben, M.P. Zetwo, M. Springer-Young, J.N. Galloway, *Geophys. Res. Lett.* **20** (1993) 699.
[136] L. Ragains, B.J. Finlayson-Pitts, *J. Phys. Chem.* **101** (1997) 1509.
[137] G. Fantechi, N.R. Jensen, O. Saastad, J. Hjorth, J. Peeters, *J. Atmos. Chem.* **31** (1998) 247.
[138] E. Canosa-Mas, H.R. Hutton-Squire, M.D. King, D.J. Stewart, K.C. Thompson, R.P. Wayne, *J. Atmos. Chem.* **34** (1999) 163.
[139] A. Notario, G. Le Bras, A. Mellouki, *Chem. Phys. Lett.* **281** (1997) 421.
[140] Y. Bedjanian, G. Laverdet, G. Le Bras, *J. Phys. Chem.* **102** (1998) 953.
[141] W. Lei, R. Zhang, *J. Chem. Phys.* **113** (2000) 153.
[142] W. Lei, D. Zhang, R. Zhang, L.T. Molina, M.J. Molina, *Chem. Phys. Lett.* **357** (2002) 45.
[143] P. Brana, J.A. Sordo, *J. Am. Chem. Soc.* **123** (2001) 10348.

[144] W. Lei, R. Zhang, L.T. Molina, M.J. Molina, *J. Phys. Chem.* **106** (2002) 6415.
[145] I. Suh, R. Zhang, *J. Phys. Chem.* **104** (2000) 6590.
[146] D. Zhang, R. Zhang, D.T. Allen, *J. Chem. Phys.* **118** (2003) 1794.
[147] J. Fan, J. Zhao, R.Y. Zhang, *Chem. Phys. Lett.* **411** (2005) 1.
[148] V.M. Ramirez-Ramirez, J. Peiro-Garcıa, I. Nebot-Gil, *Chem. Phys. Lett.* **391** (2004) 152.
[149] A.M. Winer, A.C. Lloyd, K.R. Darnall, J.N. Pitts, *J. Phys. Chem.* **80** (1976) 1635.
[150] R. Atkinson, S.M. Aschmann, J.N. Pitts, *Int. J. Chem. Kinet.* **18** (1986) 287.
[151] T.E. Kleindienst, G.W. Harris, J.N. Pitts, *Environ. Sci. Technol.* **16** (1982) 844.
[152] J. Gill, R.A. Hites, *J. Phys. Chem. A* **106** (2002) 2538.
[153] J. Peeters, L. Vereecken, G. Fantechi, *Phys. Chem. Chem. Phys.* **3** (2001) 5489.
[154] J. Arey, R. Atkinson, S.M. Aschmann, *J. Geophys. Res.* **95** (1990) 18539.
[155] S. Hatakeyama, K. Izumi, T. Fukuyama, H. Akimoto, N. Washida, *J. Geophys. Res.* **96** (1991) 947.
[156] H. Hakola, J. Arey, S. Aschmann, R. Atkinson, *J. Atmos. Chem.* **18** (1994) 75.
[157] C. Vinckier, F. Compernolle, A. Saleh, M.N. Van Hoof, I. Van Hees, *Fresenius Environ. Bull.* **7** (1998) 361.
[158] B. Nozière, I. Barnes, K.-H. Becker, *J. Geophys. Res.* **104** (1999) 23645.
[159] A. Wisthaler, N.R. Jensen, R. Winterhalter, W. Lindinger, J. Hjorth, *Atmos. Environ.* **35** (2001) 6181.
[160] R. Larsen, D. di Bella, M. Glasius, R. Winterhalter, N.R. Jensen, J. Hjorth, *J. Atmos. Chem.* **38** (2001) 231.
[161] S.M. Aschmann, R. Atkinson, J. Arey, *J. Geophys. Res.* **107** (2002), doi:10.1029/2001JD001098.
[162] V. Librando, G. Tringali, *J. Environ. Manage.* **75** (2005) 275.
[163] G. Fantechi, L. Vereecken, J. Peeters, *Phys. Chem. Chem. Phys.* **4** (2002) 5795.
[164] P.J. Lewis, K.A. Bennett, J.N. Harvey, *Phys. Chem. Chem. Phys.* **7** (2005) 1643.
[165] R. Atkinson, S.M. Aschmann, *J. Atmos. Chem.* **16** (1993) 337.
[166] S.A. McKeen, T. Gierczak, J.B. Burkholder, P.O. Wennberg, T.F. Hanisco, E.R. Keim, R.-S. Gao, S.C. Liu, A.R. Ravishankara, D.W. Fahey, *Geophys. Res. Lett.* **24** (1997) 3177.
[167] K.-H. Wohlfrom, T. Hauler, F. Arnold, H. Singh, *Geophys. Res. Lett.* **26** (1999) 2849.
[168] S.M. Aschmann, A. Reissell, R. Atkinson, J. Arey, *J. Geophys. Res.* **103** (1998) 25553.
[169] A. Reissell, C. Harry, S.M. Aschmann, R. Atkinson, J. Arey, *J. Geophys. Res.* **104** (1999) 13869.
[170] J.J. Orlando, B. Nozière, G.S. Tyndall, G.E. Orzechowska, S.E. Paulson, Y. Rudich, *J. Geophys. Res.* **105** (2000) 11561.
[171] L. Vereecken, J. Peeters, *J. Phys. Chem. A* **104** (2000) 11140.
[172] T.S. Dibble, *J. Am. Chem. Soc.* **123** (2001) 4228.
[173] M. Capouet, J. Peeters, B. Noziere, J.-F. Muller, *Atmos. Chem. Phys.* **4** (2004) 2285.
[174] S. Hatakeyama, K. Izumi, T. Fukuyama, H. Akimoto, *J. Geophys. Res.* **94** (1989) 13013.
[175] D. Grosjean, E.L. Williams, E. Grosjean, J.M. Andino, J.H. Seinfeld, *Environ. Sci. Technol.* **27** (1993) 2754.
[176] T. Hoffmann, R. Bandur, U. Marggraf, M. Linscheid, *J. Geophys. Res.* **103** (1998) 25569.
[177] R. Winterhalter, P. Neeb, D. Grossmann, A. Kolloff, O. Horie, G. Moortgat, *J. Atmos. Chem.* **35** (2000) 165.
[178] W. Hoppel, J. Fitzgerald, G. Frick, P. Caffrey, L. Pasternack, D. Hegg, S. Gao, R. Leaitch, N. Shantz, C. Cantrell, T. Albrechcinski, J. Ambrusko, W. Sullivan, *J. Geophys. Res.* **106** (2001) 27603.
[179] Y. Iinuma, O. Boge, T. Gnauk, H. Herrmann, *Atmos. Environ.* **38** (2004) 761.
[180] D. Zhang, R.Y. Zhang, *J. Chem. Phys.* **122** (2005) Art. No. 114308.
[181] T. Berndt, O. Boge, *J. Chem. Soc. Faraday Trans.* **93** (1997) 3021.
[182] M. Hallquist, I. Wangberg, E. Ljungstrom, I. Barnes, K.H. Becker, *Environ. Sci. Technol.* **33** (1999) 553.
[183] B. Bonn, G.K. Moortgat, *Amos. Chem. Phys.* **2** (2002) 183.
[184] M. Spittlera, I. Barnes, I. Bejan, K.J. Brockmann, Th. Benter, K. Wirtz, *Atmos. Environ.* **40** (2006) S116.
[185] N. Carrasco, M.T. Rayez, J.C. Rayez, J.F. Doussin, *Phys. Chem. Chem. Phys.* **8** (2006) 3211.
[186] Q.K. Timerghazin, P.A. Ariya, *Phys. Chem. Chem. Phys.* **3** (2001) 3981.
[187] V.M. Ramirez-Ramirez, I. Nebot-Gil, *Chem. Phys. Lett.* **409** (2005) 23.
[188] M. Fernandez, C. Williams, R.S. Mason, B.J.C. Cabral, *J. Chem. Soc. Faraday Trans.* **94** (1998) 1427.
[189] M. Clericuzio, G. Alagona, C. Ghio, L. Toma, *J. Org. Chem.* **65** (2000) 6910.
[190] J.A. Pople, *R&D Mag.* **41** (1999) 44.